CFD-based hydrodynamic analyses of ship course keeping control and turning performance in irregular waves

Daejeong Kim *, Tahsin Tezdogan

Department of Naval Architecture, Ocean and Marine Engineering, University of Strathclyde, 100 Montrose Street, Glasgow, G4 0LZ, United Kingdom

A B S T R A C T

Ship manoeuvrability studies are usually carried out in calm and regular seas; however, an irregular sea state can better present the real operational conditions at sea, compared to both calm and regular seas. In this study, the manoeuvrability of a well-known benchmarking ship in an irregular sea state was investigated using a fully nonlinear unsteady RANS model. The JONSWAP spectrum was used to generate long-crested irregular seas with a significant wave height of 5m and a peak period of 12.4s in full scale, representing sea state 6. Comparisons with the ship manoeuvrability in both calm and regular seas were also made with a view to identifying the changes in the manoeuvring characteristics of the ship. The generated regular waves were characterised by the height and period equivalent to the average height and period of the irregular waves applied in this work. The ship is equipped with a single propeller with a semi-balanced horn rudder, and the propeller is simulated by an actuator disk model based on the body force method. In analysing the correlations between the ship manoeuvrability and the irregular waves, the findings of this study have demonstrated that the irregular waves may cause substantial changes in the course keeping capability and turning performance when compared to the inherent manoeuvring qualities in calm water. It is expected that the results of this work can provide a deeper insight into ship manoeuvrability in irregular waves as well as help masters and navigation officers in decision-making for ship handling actions in real sea states.

1. Introduction

It has been shown that over 40% of marine incidents are related to navigational casualties from collision and grounding (EMSA, 2020). Such casualties are dominantly due to inappropriate ship manoeuvres being highly dependent on the decision of a navigation watch officer, thus highlighting the importance of understanding the manoeuvring behaviour of a ship in a real seaway. A sufficient understanding of a ship's manoeuvrability plays a central role in safe ship handling. It is true that there have been voluminous studies focusing on ship manoeuvrability in calm water in line with the recommendation of the International Maritime Organisation (IMO, 2002b), which can to some extent be used to understand the inherent manoeuvrability of a ship. However, the increasing number of navigational incidents has made it essential and urgent that the manoeuvring performance of a ship in real sea states should be studied in detail. Given that the realistic ocean waves in which a vessel navigates are mostly irregular, namely random seas, it is highly believed that the manoeuvring capability of a ship in irregular waves should be extensively investigated to improve

understanding of ship manoeuvrability in real sea states. Without a doubt, irregular waves can lead to substantial changes in the manoeuvring performance of a ship compared to that in calm water, which is closely associated with navigational safety at sea. For this reason, this study aims to analyse the manoeuvrability of a ship in an irregular seaway.

The manoeuvring behaviour of a ship is predicted by direct or indirect methods (Hasanvand and Hajivand, 2019). The direct approaches include conducting free-running model experiments in a manoeuvring basin or simulating free-running manoeuvres by means of Computational Fluid Dynamics (CFD). In the direct methods, one can provide highly reliable information about the manoeuvrability of a ship since it is considered the closest way to mimic real operating conditions. The indirect approaches are based on solving simplified mathematical models such as Abkowitz model (Abkowitz, 1964) and Manoeuvring Modelling Group (MMG) model (Inoue et al., 1981; Yasukawa and Yoshimura, 2015). While the indirect method has a significant advantage in terms of computation time, numerous integral coefficients need to be determined before solving the ship motion equations, which can be

obtained from captive model tests. The accuracy of the indirect approach is highly dependent on the range of validity of the hydrodynamic derivatives, limiting the applicability of these indirect methods. Moreover, these simplified mathematical models are not capable of precisely resolving the complex hull/propeller/rudder interactions critical to estimate the manoeuvring performance of a ship. Given this, the direct approach instead of the indirect method seems the most adequate option for a more accurate estimation of ship manoeuvring performance.

Free running CFD simulations, i.e., the direct approach, are rapidly gaining popularity with ever-increasing computing power and efficient numerical algorithms. The CFD-based simulations are easily capable of incorporating both viscous and nonlinear effects in the flow and free surface, which is considered significant for manoeuvring problems. In this regard, Reynolds-Averaged Navier-Stokes (URANS) or Detached Eddy Simulation (DES) based CFD methods have been very attractive alternatives to the indirect approach. Furthermore, in comparison with traditional experiments, using the CFD approach can also be advantageous for not only reducing cost, time, and labour but also providing the detailed local flow physics of interest, such as around stern.

In one of the first studies in this field, Mofidi and Carrica (2014) presented free-running simulations of zigzag manoeuvres of the KCS model in deep, calm water, utilising CFDShip-Iowa, which is a piece of general-purpose CFD software developed at the University of Iowa. In their work, the CFD results were validated against the available experimental data, and the comparisons were highly satisfactory, demonstrating the reliability of the direct CFD approach. Carrica et al. (2016) extended the free-running simulations from deep water to shallow water for zigzag manoeuvres for the KCS, and the results obtained using the direct CFD method agreed well with the experimental results. Likewise, some other researchers attempted to investigate the manoeuvring performance of ships for the calm water condition by performing free-running CFD simulations (Broglia et al., 2015; Shen et al., 2015; Dubbioso et al., 2016; Wang et al., 2016; Hasanvand and Hajivand, 2019).

The Marine Environment Protection Committee (MEPC) of the IMO adopted the interim guidelines for determining minimum propulsion power to maintain the manoeuvrability of ships in adverse conditions which is specifically concerned with the course keeping capability in waves (IMO, 2014). Following this, a specialist committee responsible for the manoeuvring performance of ships in waves was formed by the 29th International Towing Tank Conference (ITTC, 2017b). As noted, recent trends in ship manoeuvres show an increasing demand for accurately evaluating a ship's manoeuvrability in waves, attracting more attention from academic researchers. In keeping with this trend, free-running CFD models have begun to take into account the presence of waves, as coupled with the Stokes wave models. Wang et al. (2017) performed the direct simulations of course keeping manoeuvres for the ONR Tumblehome ship model in both calm water and regular waves using naoe-FOAM-SJTU, which is a CFD solver developed on the open-source platform OpenFOAM. The predicted results matched satisfactorily with the benchmark data in Tokyo 2015 CFD Workshop in ship hydrodynamics. Following this, free-running simulations of the ONR Tumblehome ship in regular waves were further carried out for zigzag manoeuvres (Wang et al., 2018) and standard turning circle manoeuvres (Wang and Wan, 2018), utilising the same CFD code. Kim et al. (2021c) performed simulations of course keeping and turning circle manoeuvres in regular waves with variations in wave directions using a RANS solver for the KCS model with a moving rudder and a rotating actuator disk. The CFD results were compared with available experimental data and showed good agreement. They also examined spatial and temporal convergence analyses which showed that monotonic convergence was achieved for the results. Then, a series of studies on the manoeuvrability of the KCS model have been performed, such as course keeping and turning circle manoeuvres in regular waves of different wavelengths (Kim et al., 2021a) and different wave heights (Kim et al., 2021b). They

further evaluated the effects of the propulsion failure on the manoeuvrability of the KCS model in regular waves using a fully nonlinear unsteady RANS model (Kim et al., 2022).

As stated previously, irregular waves can better represent realistic sea states. Nevertheless, to date, only a few remarkable studies have been devoted to investigating the effect of irregular waves on the manoeuvrability of ships. Hasnan et al. (2019) performed a series of free-running experiments to estimate the turning behaviour of the KCS and KVLCC2 in short-crested irregular head seas. Their key findings showed that irregular head seas led to substantial changes in the turning capabilities of ships including critical turning indices, compared to the calm water case. In this regard, the findings from the study by Hasnan et al. (2019) raised further questions about course-keeping and turning capabilities of a ship in irregular waves of different directions. The reason for this question can be explained by the fact that Kim et al. (2021c) demonstrated the manoeuvring behaviour of a ship depends highly on the wave propagation directions. In particular, the investigation in Kim et al. (2021c) showed course-keeping abilities can be clearly identified in oblique waves, causing a large deviation from the planned route. The effect of wave direction on the manoeuvring performance was studied earlier by Kim et al. (2021c); however, their study was only performed in regular waves. Therefore, it is crucial to evaluate the manoeuvrability of a ship in irregular waves of different directions as well to have better understanding of the ship's manoeuvring properties in an irregular seaway.

Given this background, the study reported in this paper was motivated to predict the manoeuvrability of a ship in irregular head and oblique bow seas, using the direct CFD method capable of resolving all physics involved in the manoeuvre. To the best of our knowledge, there has been no specific study in the literature up to now focusing on the manoeuvrability of a ship in irregular head and oblique seas, except for the turning ability in irregular head seas. It is also expected that the free-running CFD simulations can help to gain insights into the hydrodynamic characteristics occurring during the manoeuvre by providing the visualisation of the flow field. This study therefore aims to develop a comprehensive understanding of the manoeuvring behaviour of a ship in real sea states.

In this paper, a study of free-running manoeuvres for the KCS container ship was performed in irregular waves, including course-keeping and turning circle manoeuvres, based on the RANS based CFD method. Free-running manoeuvres in both calm water and regular waves were also carried out, with a view to identifying the changes in the ship manoeuvrability in different environmental conditions. During free-running simulations, self-propulsion conditions were firstly achieved to reach the approach speeds. Then, course-keeping manoeuvres from the stable state of self-propulsion condition were executed to evaluate the steering capability under different wave conditions. Finally, the turning qualities of the ship were assessed by performing standard turning circle manoeuvres.

The remaining paper is framed as follows: Section 2 presents the research methodology of the free-running CFD simulation, with details provided in the contained sub-sections. In Section 3, the CFD results obtained from the manoeuvring simulations (such as course-keeping and turning circle manoeuvres) are illustrated in detail. Finally, conclusions drawn from this work are discussed in Section 4, along with recommendations for future avenues of study.

2. Methodology

This section will describe the research methodology used in detail. The process of examining the manoeuvring qualities of the ship is divided into four main steps: *1) goal and scope, 2) numerical modelling, 3) free running simulations, and 4) result of analysis*. The major characteristics of each step are presented in Fig. 1. The first step deals with the research aim and objectives with an outline of the scope of the study to achieve them. The second step presents the details of the numerical
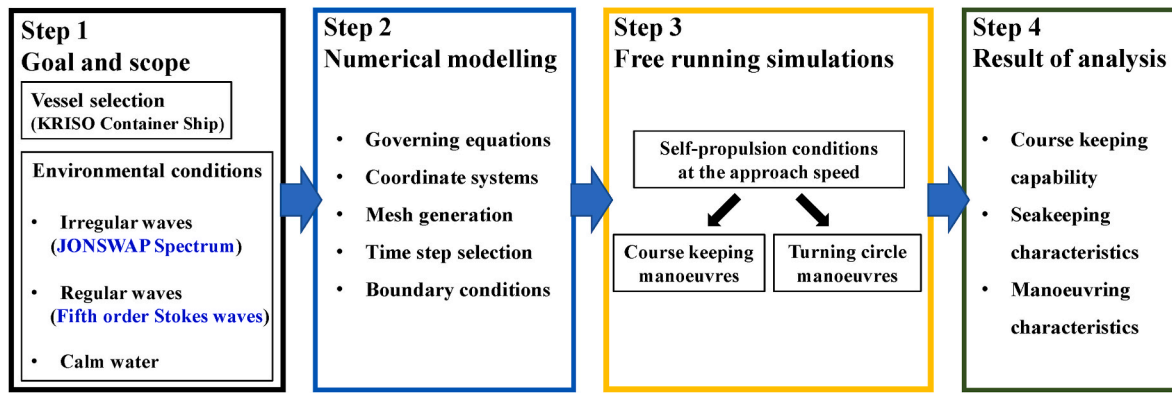
Step 1 Goal and scope	Step 2 Numerical modelling	Step 3 Free running simulations	Step 4 Result of analysis
Vessel selection (KRISO Container Ship) **Environmental conditions** • Irregular waves (**JONSWAP Spectrum**) • Regular waves (**Fifth order Stokes waves**) • Calm water	• Governing equations • Coordinate systems • Mesh generation • Time step selection • Boundary conditions	Self-propulsion conditions at the approach speed Course keeping / Turning circle manoeuvres / manoeuvres	• Course keeping capability • Seakeeping characteristics • Manoeuvring characteristics

Fig. 1. Flow chart showing the methodology adopted in the study.

methods applied to the free-running CFD model, including governing equations, mesh generation, time step selection, etc. The manoeuvre procedure used in the simulation was discussed in the third step, which also includes detailed descriptions of two representative free-running manoeuvres: course-keeping and turning manoeuvres. In the fourth step, the results from this study were analysed with particular emphasis on course-keeping, seakeeping, and turning characteristics which were thought to be closely associated with navigational safety at sea. Each step will be further detailed in the following sub-sections (2.1–2.4).

2.1. Step 1: goal and scope

The overall aim of this paper was to contribute to enhancing navigational safety at sea, providing a better understanding of the manoeuvrability of a ship in a real seaway. The specific objectives of this study are as follows:

(1) To develop the free-running CFD model for ship manoeuvres in irregular waves
(2) To examine the manoeuvring behaviour of the ship during course keeping and turning manoeuvres in irregular waves, along with comparisons with the ship manoeuvrability in both calm and regular seas
(3) To identify the critical manoeuvring parameters which could help navigation officers determine appropriate decision making for ship handling in real sea states to avoid collision incidents
(4) To recommend future studies to obtain a comprehensive understanding of the ship manoeuvrability at sea. This research is

expected to be used as a guide for exploring extended scopes while investigating limitations identified by this paper.

A 1/75.24 scale model of the KCS appended with a semi-balanced rudder and an actuator disk has been used within this study. The views of the KCS model are shown in Fig. 2, and the main properties of the model are listed in Table 1. The cases to be simulated in CFD are shown in Table 2 and Fig. 3. Course keeping and turning manoeuvres were carried out in five environmental conditions, each identified by their case numbers: *1) irregular head sea, 2) irregular bow sea, 3) regular*

Table 1
Principal particulars of the KCS.

| Main particulars	Symbols	Model scale (1:75.24)
Length between the perpendiculars	L_{BP} (m)	3.057
Length of waterline	L_{WL} (m)	3.0901
Beam at waterline	B_{WL} (m)	0.4280
Draft	D (m)	0.1435
Displacement	Δ (m^3)	0.1222
Block coefficient	C_B	0.651
Ship wetted area with rudder	S (m^2)	1.6834
Longitudinal centre of buoyancy	% $L_{BP,}$ fwd+	−1.48
The metacentric height	GM (m)	0.008
Radius of gyration	K_{xx}/B	0.49
Radius of gyration	K_{yy}/L_{BP}, K_{zz}/ L_{BP}	0.25
Propeller diameter	D_P (m)	0.105
Propeller rotation direction (view from stern)		Right handed side
Rudder turn rate	(deg./s)	20.1
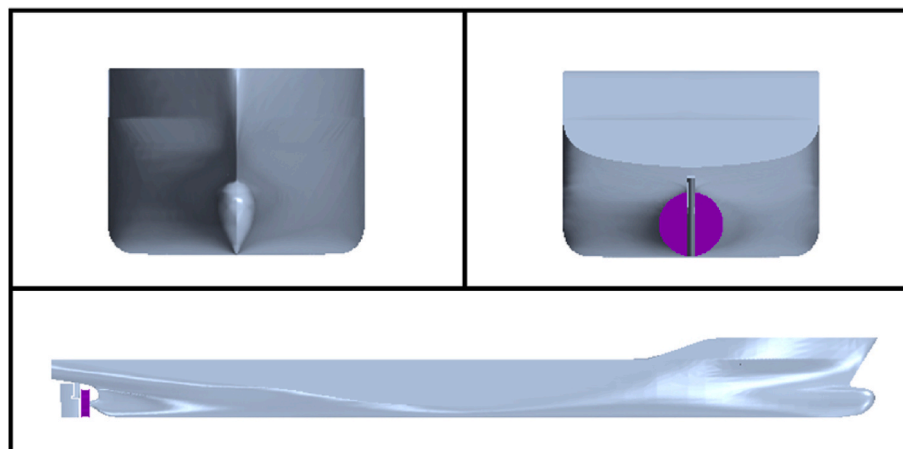
Fig. 2. KCS geometry with a semi balanced rudder and an actuator disk.

Table 2
The simulation cases to which the CFD model is applied.

Property	Case no.				
	1	2	3	4	5
Environmental condition	Irregular wave (JONSWAP Spectrum)	Irregular wave (JONSWAP Spectrum)	Regular wave (5th-order Stokes wave)	Regular wave (5th-order Stokes wave)	Calm sea
Significant wave height H_s(m)	0.0665 (5.0 m in full scale)	0.0665 (5.0 m in full scale)	–	–	–
Peak period T_p(s)	1.43 (12.4 s in full scale)	1.43 (12.4 s in full scale)	–	–	–
Average wave height $\overline{H}$(m)	0.0407 (3.06 m in full scale)	0.0407 (3.06 m in full scale)	0.0407 (3.06 m in full scale)	0.0407 (3.06 m in full scale)	–
Average wave period $\overline{T}$(s)	1.20 (10.41 s in full scale)	1.20 (10.41 s in full scale)	1.20 (10.41 s in full scale)	1.20 (10.41 s in full scale)	–
Approach speed U_0(m/s)	0.925	0.943	0.989	0.945	1.094
Propeller rev. (RPS)	13.38	13.38	13.38	13.38	13.38
Encounter angle μ(degrees)	180 (head sea)	225 (bow sea)	180 (head sea)	225 (bow sea)	–
Encounter Freq. f_e (Hz)	–	–	1.276	1.129	–

head sea, 4) regular bow sea, and 5) calm sea. It should be reiterated that self-propulsion conditions were firstly achieved prior to such manoeuvres. As for the irregular wave conditions (Cases 1 and 2), the JONSWAP spectrum was used to generate long-crested irregular seas with a significant wave height of 0.0665m and a peak period of 1.43s in model scale. These values correspond to a significant wave height of 5m and a peak period of 12.4s in full scale, representing sea state 6. It is worth noting that sea state 6 is characterised by "very rough seas" by the World Meteorological Organisation, almost consistent with the adverse conditions defined by IMO (2021). Sea state 6 was thus adopted in this study in response to a rapidly increasing demand for the evaluation of ship manoeuvrability in adverse sea conditions. Regarding regular wave cases, regular waves were characterised by a wave height and period equal to the average height and period of the irregular waves applied in this study for meaningful comparisons of the results. The free-running manoeuvres in calm water were also carried out to address the inherent manoeuvring qualities of the ship. Note that all free-running simulations were performed using deep water conditions.

2.2. Step 2: numerical modelling

In this study, the free-running manoeuvres of the KCS were simulated with the commercial CFD software STAR-CCM+, version 15.04. A detailed explanation of the numerical setup for the present CFD model is given in the following sub-sections.

2.2.1. Governing equations

An Unsteady Reynolds-Averaged Navier-Stokes (URANS) method was used to solve the governing equations suited for describing unsteady turbulent incompressible flows around a ship. In RANS equations, the flow parameters are decomposed into fluctuating and time-averaged quantities, using the Reynolds decomposition principle (Reynolds, 1895). The averaged continuity and momentum equations for unsteady incompressible flows are written in tensor notation and Cartesian coordinates as follows (Ferziger and Peric, 2020):

$$\frac{\partial(\rho \overline{u}_i)}{\partial x_i} = 0 \tag{1}$$

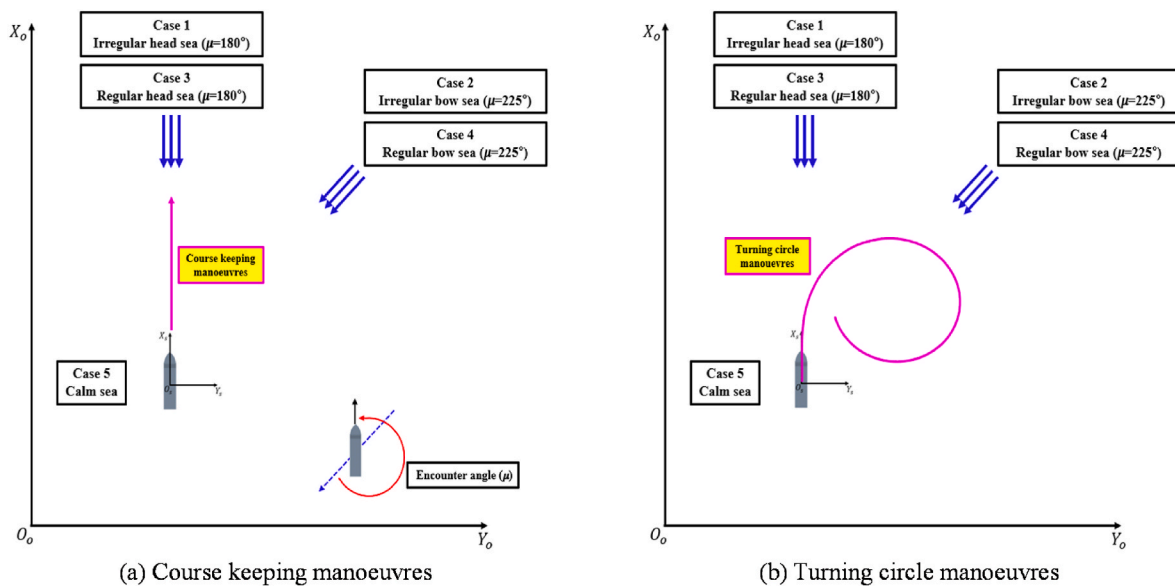(a) Course keeping manoeuvres
(b) Turning circle manoeuvres

Fig. 3. Schematic views of the simulation cases applied to this study, (a) course keeping manoeuvres (b) turning circle manoeuvres.

$$\frac{\partial(\rho\overline{u}_i)}{\partial t} + \frac{\partial}{\partial x_j}\left(\rho\overline{u}_i\overline{u}_j + \rho\overline{u_i'u_j'}\right) = -\frac{\partial\overline{p}}{\partial x_i} + \frac{\partial\overline{\tau}_{ij}}{\partial x_i} \tag{2}$$

where ρ is the fluid density, $\overline{u}_i$ is the averaged velocity vector, x_i (i = 1, 2, 3) are the Cartesian coordinates, $\rho\overline{u_i'u_j'}$ is the Reynolds stresses, $\overline{p}$ is the mean pressure and $\overline{\tau}_{ij}$ are the mean viscous stress tensor components. This stress tensor for a Newtonian fluid can be shown in Eq. (3)

$$\overline{\tau}_{ij} = \mu\left(\frac{\partial\overline{u}_i}{\partial x_j} + \frac{\partial\overline{u}_j}{\partial x_i}\right) \tag{3}$$

in which μ means the dynamic viscosity.

The solver employed uses a finite volume method (FVM) which discretises the integral formulation of the Navier-Stokes equations for numerical computations of incompressible viscous flows. The temporal discretisation of the transient terms was based on a second-order implicit backward Euler scheme. A second-order upwind scheme and a second-order centred scheme were used for the spatial discretisation of the convection terms and the diffusive terms, respectively. SIMPLE (Semi-Implicit Method for Pressure-Linked Equations) algorithm was adopted for the pressure-velocity coupling.

2.2.2. Physics modelling

In this study the three-dimensional RANS equations were solved with the Shear Stress Transport (SST) model (Menter, 1994) as a turbulence closure model. This turbulence model is based on a blending of a $k-\omega$ model used near the wall and a $k-\varepsilon$ model used in the far-field. It has been demonstrated that Menter's SST model provides accurate predictions of flows with strong adverse pressure gradients and separation (Menter et al., 2003), which is of particular importance in ship manoeuvring studies. Turbulence modelling has been shown to be one of the main factors in obtaining accurate predictions of complex flows (Terziev et al., 2019). Along with the SST turbulence model, the all-y + wall treatment was used to obtain mean flow properties (such as pressure, velocity, and separation) in turbulent boundary layers. This wall treatment is a hybrid treatment that attempts to emulate the low-y + wall treatment for fine meshes (when the wall y+ <5), and the high-y + wall treatment for coarse meshes (when the wall y+ >30). The Volume of Fluid (VOF) approach was adopted as an interface-resolving method in which the air-water interface is tracked by the volume fraction in each cell. In order to simulate the realistic motion of the free-running ship, the current CFD model utilised the Dynamic Fluid Body Interaction (DFBI) module integrated into a 6 DOF solver. The 6 DOF motion solver computes hydrodynamic forces and moments acting on the ship and then solves the governing equations of motion to obtain kinematic characteristics of the ship. With the aim of resolving the flow field interaction between the ship hull and the propeller, an infinite-blade actuator disk was modelled based on the body force method adding momentum to the flow and forces to the ship. The modelling of the actuator disk requires numerous input variables that need to be obtained from experiments. The input parameters were selected based on the propeller experimental results performed by Hiroshima University (SIMMAN, 2020). The present propeller disk model has been proven to be reliable in assessing the ship manoeuvrability, as validated in the authors' previous work (Kim et al., 2021c).

The irregular waves generated in the numerical simulation (Case 1 and 2) were based on the JONSWAP spectrum, which was derived from fetch-limited observations made in the North Sea and described by Hasselmann et al. (1973). The JONSWAP formulation used in this analysis can be expressed as follows:

$$S_J(\omega) = A_\gamma S_{PM}\left(\omega\right)\gamma^{\exp\left(-0.5\left(\frac{\omega-\omega_p}{\sigma\omega_p}\right)^2\right)} \tag{4}$$

$$A_\gamma = 1 - 0.287\ln(\gamma) \tag{5}$$

$$S_{PM}(\omega) = \frac{5}{16}\left(H_s^2\omega_p^4\right)\omega^{-5}\exp\left(-\frac{5}{4}\left(\frac{\omega}{\omega_p}\right)^{-4}\right) \tag{6}$$

$$\sigma = \begin{cases} 0.07 & (\omega \le \omega_p) \\ 0.09 & (\omega > \omega_p) \end{cases} \tag{7}$$

where ω and ω_p represent the incident wave frequency and modal wave frequency, respectively. A_γ is the normalising factor with γ referring to the non-dimensional peak-enhancement factor (γ =3.3). $S_{PM}(\omega)$ is the Pierson-Moskowitz spectrum, H_s is the significant wave height, and σ denotes the spectral width parameter.

It should also be noted that a fifth-order Stokes wave model was used for generating the regular waves (Case 3 and 4) in accordance with the theory of the fifth-order Stokes wave theory proposed by Fenton (1985). The reason for selecting the fifth-order Stoke wave was to simulate more realistic wave profiles. According to Siemens (2020), the wave which is modelled with a fifth-order approximation to the Stokes theory of waves more closely resembles a real wave than one generated by the first-order approximation.

2.2.3. Coordinate systems

Fig. 4 illustrates different coordinate frames defined in the present CFD model: *(1) Earth-fixed coordinate ($O_o - X_oY_oZ_o$), (2) Ship-fixed coordinate (o_s - $x_sy_sz_s$), 3) Propeller-fixed coordinate (o_p - $x_py_pz_p$), and (4) Rudder-fixed coordinate (o_r - $x_ry_rz_r$).* The earth-fixed coordinate is considered as an inertial frame with the origin fixed at point O_o. In this inertial frame, the governing equation for the fluid flow was solved, and the hydrodynamic pressure and shear forces and moments acting on the ship hull were calculated. Then, the forces and moments were converted to the ship-fixed coordinate system which is a moving reference system with the origin located at the ship's centre of gravity (CG), following all 6-DOF motions of the body. The body local coordinate system is used to solve the governing equations of motion for calculating the ship's velocities, which can be expressed as follows:

$$\frac{\mathrm{d}(m\mathbf{V})}{dt} = \mathbf{f} \tag{8}$$

$$\mathrm{M}_b\frac{\mathrm{d}\boldsymbol{\omega}}{\mathrm{dt}} + \boldsymbol{\omega} \times \mathrm{M}_b\,\boldsymbol{\omega} = \mathbf{m} \tag{9}$$

where m is the mass of body, $\mathbf{V}$ is the velocity vector of its centre of mass, $\mathbf{f}$ is the resultant force vector acting on the ship, M_b denotes the tensor of moments of inertia in the body-fixed coordinate system, $\boldsymbol{\omega}$ denotes the angular velocity vector of the body and $\mathbf{m}$ represents the resultant moment vector acting on the body. The resultant forces ($\mathbf{f}$) and moments ($\mathbf{m}$) acting on the ship can be written as follows (Hasanvand and Hajivand, 2019):

$$\mathbf{f} = \boldsymbol{F_p} + \boldsymbol{F_\tau} + \boldsymbol{F_g} + \sum\boldsymbol{F_{ext}} \tag{10}$$

$$\mathbf{m} = \boldsymbol{m_p} + \boldsymbol{m_\tau} + \sum\boldsymbol{m_{ext}} \tag{11}$$

with representing $\boldsymbol{F_p}$ and $\boldsymbol{m_p}$ the pressure force and moment, $\boldsymbol{F_\tau}$ and $\boldsymbol{m_\tau}$ the shear force and moment obtained by solving the flow field and the integration of the pressure and shear stress on the ship hull. $\sum\boldsymbol{F_{ext}}$ and $\sum\boldsymbol{m_{ext}}$ are the external force and moment acting on the ship, respectively, and $\boldsymbol{F_g}$ is the gravitational force exerted at the CG. The propeller thrust and torque based on the body force method were applied to the external force and moment in the current CFD simulation. Unlike pure resistance or seakeeping simulations which require only the earth-fixed and ship-fixed frames (Tezdogan et al., 2015), the propeller-fixed and rudder-fixed frames need to be additionally defined in the free-running CFD model. These frames were designed to be attached to the ship, thus
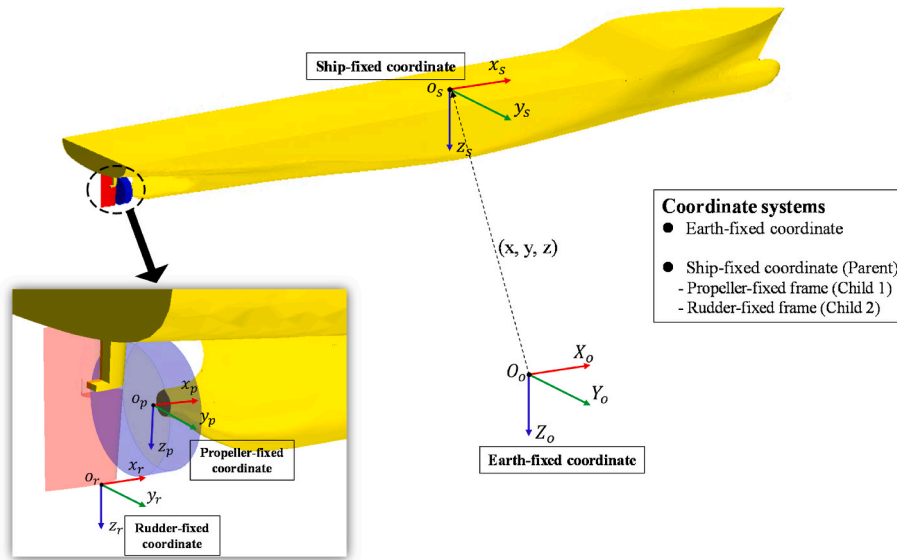
Fig. 4. The reference coordinate systems of the free-running simulation used in this study.

their relative positions with respect to the ship were not changed. The direction of the propeller thrust is determined by the propeller-fixed coordinate with the origin fixed at the centre of the disk, in which the positive x_p-axis points in the direction where the actuator disk produces thrust force. In the rudder-fixed frame, the $o_r z_r$-axis plays a role as the axis about which the rudder blade rotates, which is necessary for the course-keeping and turning circle manoeuvres. The propeller fixed reference was defined to determine the direction in which the actuator disk model produces thrust force, while the rudder-fixed frame was adopted with the aim to control the rudder movement required for the prescribed free-running manoeuvre.

2.2.4. Mesh generation

The process of mesh generation was conducted by the built-in automated meshing tool of STAR-CCM+, which uses the Cartesian cut-cell method. Three different mesh generations were applied for the free-running simulation (Case 1 and 2 - irregular waves, Case 3 and 4 - regular waves, and Case 5 - calm water), resulting in a computation mesh of circa 14, 11, and 6 million cells in total, respectively. Trimmed

hexahedral meshes were used to produce a high-quality grid for the complex domains. In order to adequately resolve the boundary layer region, the ship hull surfaces were covered with six layers of orthogonal prismatic cells by using a prism layer mesher. Prism layers refer to the region of closely packed cells near solid surfaces to capture the boundary layer. Local grid refinements were made in the vicinity of the bow, the stern, the tight gap parts between the rudder blade and horn, and the propeller wake region to ensure that the complex flows were precisely captured. In addition, a finer mesh was created in the free surface where incident waves were expected to travel in the computational domain. For the irregular wave cases (Case 1 and 2), the free surface mesh was generated following the guidelines for ship CFD applications from ITTC (2011) and the recommendations put forward by CSP (2021). According to CSP (2021), the cut-off frequency, referring to the highest wave frequency (the shortest wavelength) to be accurately resolved in the simulation, should be first selected from a wave energy spectrum. In general, cut-off frequency (f_c) to peak frequency (f_p) ratios f_c/f_p should be greater than 2 since relatively low a cut-off frequency may affect properties of resultant spectrum and values of target significant wave
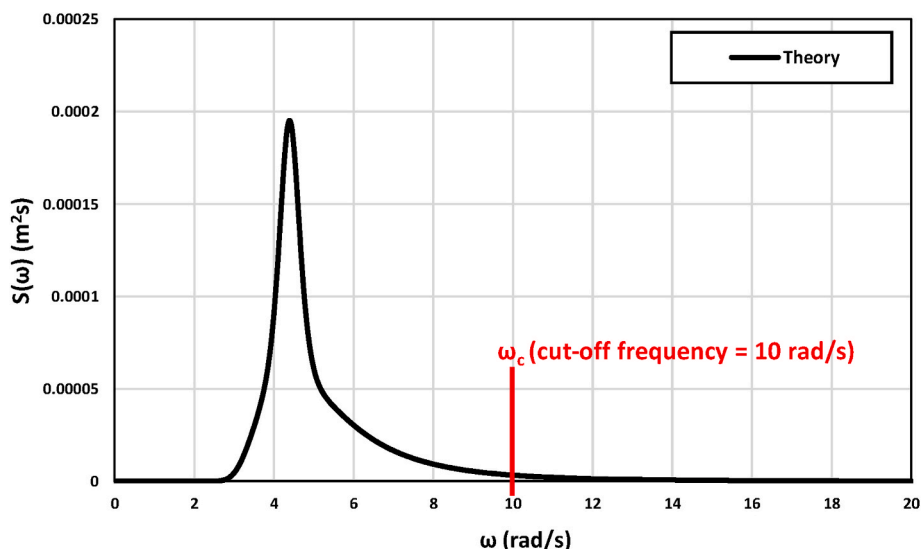

Fig. 5. The JONSWAP wave spectrum applied in this study (sea state 6, $H_s = 0.0665$m and $T_p = 1.43$s).

height and modal period (ITTC, 2017a). Accordingly, the cut-off frequency of 10 rad/s was chosen in this study, which satisfies this ratio condition (f_c/f_p =2.3), as depicted in Fig. 5. It has to be stated that the cut-off frequency to peak frequency ratio (f_c/f_p) was calculated at model scale in this study. Given the cut-off frequency selected, 20 grid points for the shortest wavelength were generated in the x and y directions (ITTC, 2011). It is important to note that a constant cell size for both x and y directions was applied in the free surface refinement region to ensure simulation stability (Romanowski et al., 2019). It should be noted that in ITTC (2011), there are no definite recommendations regarding how to generate meshes in the vertical direction for irregular waves. In this study, 30 grids points for the expected maximum wave height (1.2 times H_s) were generated in the z-direction according to CSP (2021). When it comes to the regular wave simulations, 80 cells per wavelength in the x and y directions and 20 cells per wave height in the z-direction were generated, applying a constant cell size for both x and y directions in the refined grid area for the free surface (ITTC, 2011). Fig. 6, as an example, presents the cross-sections of the final computational mesh obtained from Case 1 and 2 (the irregular wave condition). The computational domain for the present numerical model was composed of three different regions: *1) background region, 2) hull overset region, and 3) rudder blade overset region*. The latter two regions were involved in applying the dynamic overset grid technique. Using the dynamic overset mesh can be advantageous for modelling moving bodies, which enables

overset parts to move independently without any constraints while yielding a high-quality grid. The hull overset region was defined with the purpose of simulating the full 6-DOF motions of the ship during manoeuvres. The overlapping region which was tailored to the rudder blade enabled the rudder deflection based on the prescribed manoeuvring mechanism. It should be stated that the distance of the gap part between the rudder blade and the rudder horn was adjusted, aiming to obtain valid interpolations between the meshes.

2.2.5. Determination of the time step

For implicit unsteady simulations, the time step is largely determined by the flow features, rather than the Courant number (CFL) condition. To gain an accurate description of the wave propagation, two different time step resolutions were selected based on the flow properties of each simulation. For irregular wave simulations, ITTC (2011) recommends that a minimum of 60 time steps per period for the shortest waves should be used. Note that the shortest wave period can be estimated by determining the cut-off frequency, as previously seen in Fig. 5. Accordingly, the time step was chosen at 2.5×10^{-3} s for the irregular wave cases (Case 1 and 2), which is lower than that calculated from the recommendation of ITTC (2011). For the regular wave cases (Case 3 and 4), the time step was determined at 5.0×10^{-3} s, which satisfies the guidelines of ITTC (2011) where a minimum of 100 time steps per period for regular waves should be used. The time step used in the regular wave
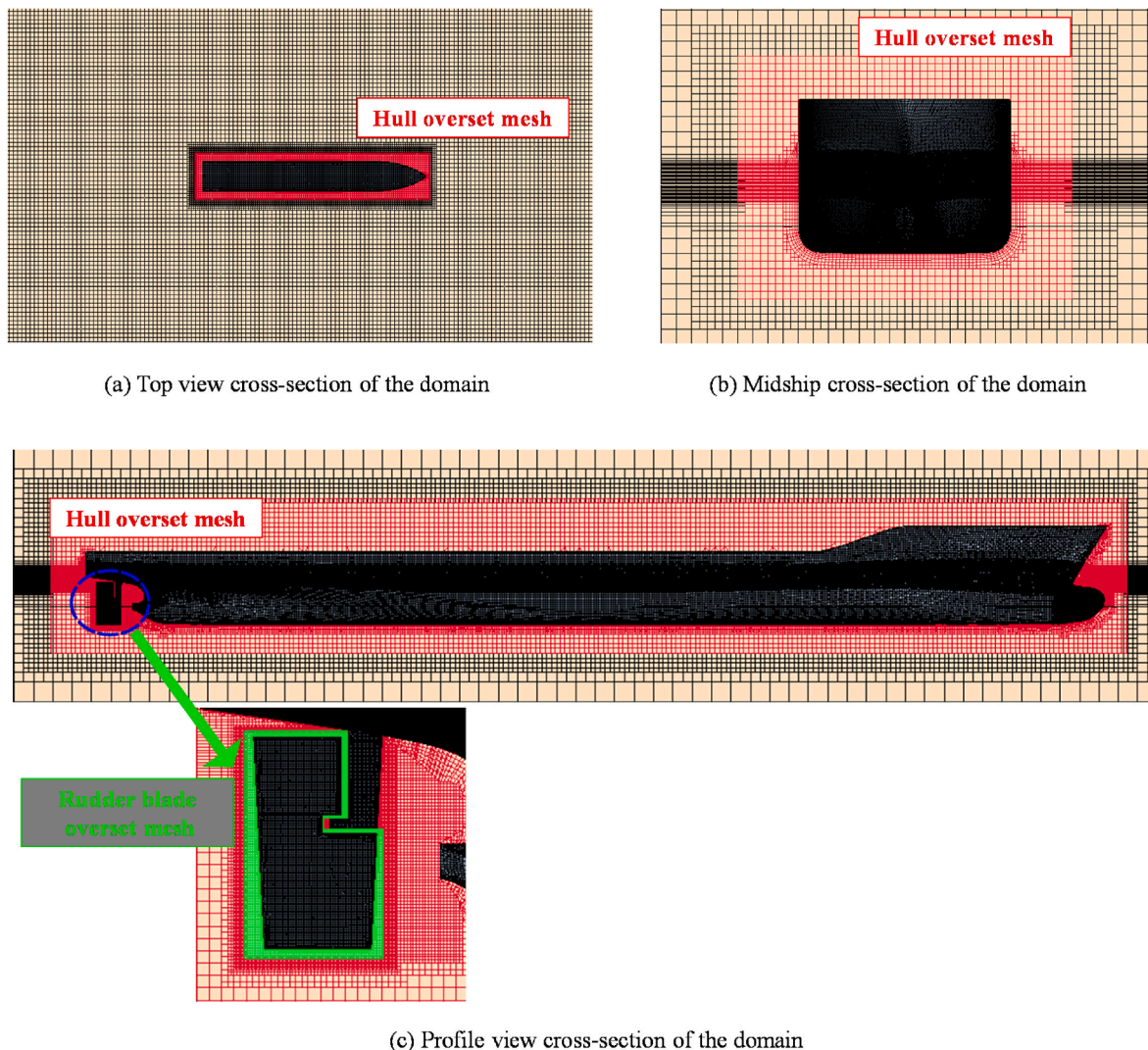

(a) Top view cross-section of the domain

(b) Midship cross-section of the domain

(c) Profile view cross-section of the domain

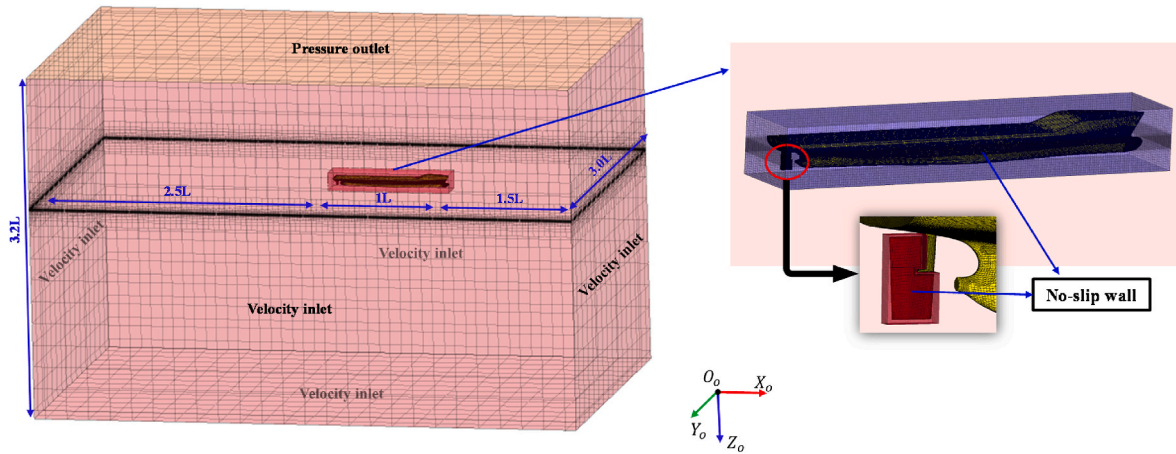**Fig. 6.** Mesh structure of the computational domain, Case 1 and 2 (Irregular wave cases).

Fig. 7. The computational domain with the imposed boundary conditions.

simulations was also applied to the calm water case (Case 5).

2.2.6. Computational domain and boundary conditions

It is of importance to define appropriate boundary conditions for numerical simulations in order to obtain reliable results, along with the quickest flow solution (Kavli et al., 2017). A schematic drawing of the computational domain with the KCS model and the notations of applied boundary conditions are presented in Fig. 7. The boundaries for the present CFD model were defined in accordance with the recommendations from CSP (2021) for similar flow problems. A velocity inlet boundary condition was set in the two opposite faces at the x-direction of the domain. The side and bottom boundaries were also modelled as a velocity inlet condition to prevent a velocity gradient from occurring between the fluid and the wall. On the top of the domain, a pressure outlet condition was applied to represent infinite air conditions. The surfaces of the moving bodies, i.e., the ship hull and the rudder blade, were set as no-slip boundary conditions. To mitigate undesired wave reflection from the boundaries, the VOF wave forcing capability of the software package was employed for the simulations in waves (Case 1–4) while the calm water simulation (Case 5) adopted the wave damping capability. Such capabilities were applied at all the vertical boundaries with a forcing/damping length equal to 1.0 L_{BP} (~3.06 m), as recommended by CSP (2021).

Three different motion capabilities were assigned for each computational region for free-running simulations, as shown in Fig. 8. The hull

overset region was free to move in all degrees of freedom by the DFBI rotation and translation module incorporated with a hierarchy of bodies. The rudder overset region which encompasses the rudder blade was defined to be a child of the ship hull (parent body), such that the rudder followed the ship during free-running manoeuvres. In addition to this, the rudder overlapping region was also designed to have rotational motions relative to the ship based on the prescribed manoeuvring module. The background region, which contains the free-surface refinement grids, was superimposed with the velocities of the ship surge, sway, and yaw motions. It is important to note that the application of other motions (namely heave, pitch, and roll) may prevent the generated waves from remaining within the refined free surface grids when the ship experiences large motions, which cannot ensure the desired wave propagation.

2.3. Step 3: free running simulations

Ship manoeuvres, such as course-keeping or turning circle tests, are generally evaluated from the stable state of self-propulsion conditions, in which the approach speed is achieved. Hence, the first stage in the present CFD simulation was to perform the self-propulsion computation before the start of the course-keeping or turning circle manoeuvres. Throughout all simulations presented in this work, the revolutions per second (RPS) of the propeller model was set to be 13.38 n/sec which is the same value as that applied for the free-running manoeuvres of the KCS in waves carried out by Kim et al. (2021c).

To assess the course-keeping capability of the ship, the course-keeping manoeuvres were performed based on the following module (Eq. (12) and (13)):

$$\delta(t) = K_p e(t) + K_i \int_0^t e(t)dt + K_d \frac{de(t)}{dt} \tag{12}$$

$$e(t) = \psi(t) - \psi_c \tag{13}$$

with $\delta(t)$ representing the rudder angle, $\psi(t)$ the instantaneous yaw angle at a given time, ψ_c the target yaw angle which was defined at 0° to keep the ship straight. K_p K_i, and K_d denote the proportional, integral, and derivative control gains, respectively. For the present CFD model, the control gains were set to $K_p = 5$, $K_i = 0.05$, and $K_d = 3$ after several trials and errors. It should be noted that the important variables related to the course-keeping ability can be significantly affected by the control gains, which imply that the good course keeping capability can be established by finding the optimal gains.

To evaluate the turning capability of the ship, the standard turning circle manoeuvres were carried out based on the control function given
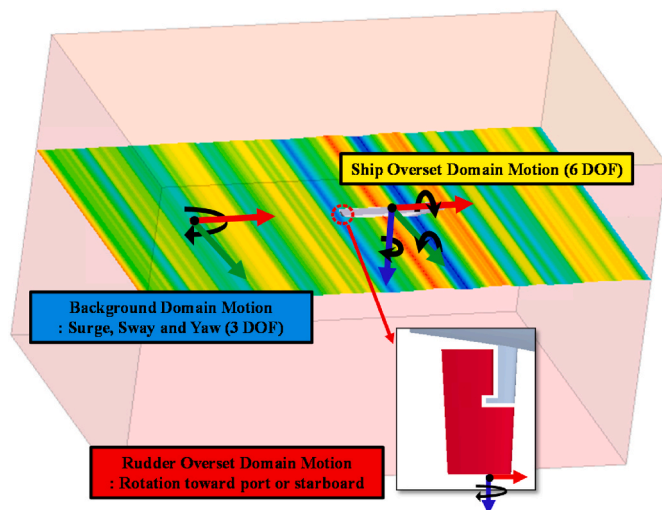

Fig. 8. The view of the motions of the generated domains.

in Eq. (14):

$$\delta(t) = \begin{cases} \max(0, \, kt), \; \delta \le 35 \\ 35 \end{cases} \qquad (14)$$

where k is the maximum rudder rate. In this work, the maximum rudder rate was selected to be $k = 20.1°/s$ (which corresponds to a full-scale rate of $2.32°/s$). The turning circle manoeuvres, as the equation suggests, deflect the rudder to a maximum 35-degree angle, which is kept constant until the ship completes the turning manoeuvre.

2.4. Step 4: results of analysis

In line with the methodology provided in Step 3, the present study carried out the free-running simulations to examine the manoeuvring performance of the ship in irregular waves. The comparison of the manoeuvring results in irregular waves to those in calm and regular seas was made with the aim of identifying the changes in the ship's manoeuvrability in irregular waves.

3. Case studies (results of step 4)

3.1. Validation and verification

It is important to ensure that the number of waves encountered should be large enough during the computation for accurately calculating the statistical characteristics of irregular seas. ITTC (2017a) recommends that a minimum of 50 waves should be encountered for model scale tests in the presence of irregular waves, while further highlighting encountering 100 waves is preferred for the resultant values of the significant wave height and modal period. Since the selection of encountering 100 waves requires a significantly high run time, the present study complied with the minimum requirement (50 waves) for the validation of irregular wave generation to compromise the computational resources and accuracy. It is worth noting that it is technically difficult to record the wave elevation at a fixed point in the present free-running simulation because of the moving computational domain. Alternatively, an additional simulation was performed by generating the static background domain (without hull and rudder grids) with the same background grids used for the manoeuvring simulation. In the simulation, the wave elevation was recorded using the wave probe located 1.20 L_{BP} in front of the ship to monitor the irregular waves generated. Fig. 9 shows the time history of the wave elevation recorded by the probe. The Fast Fourier Transform (FFT) was applied to the time series of the wave
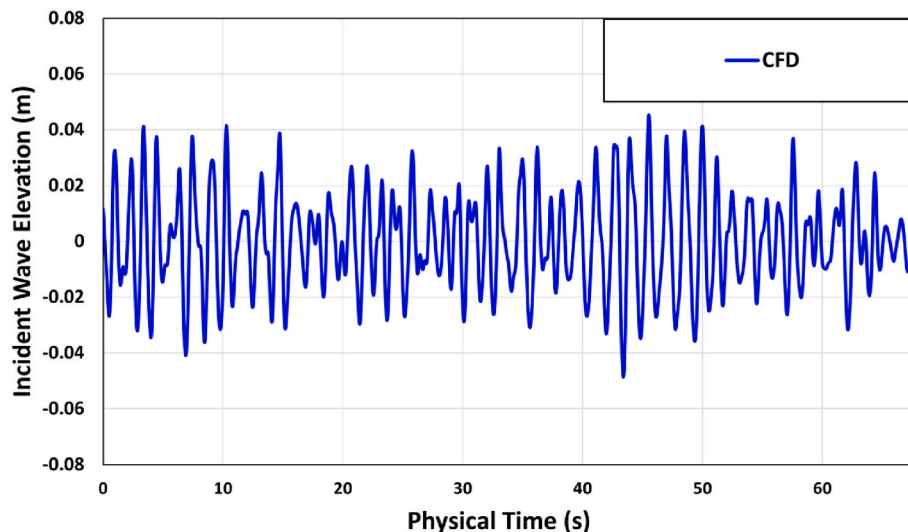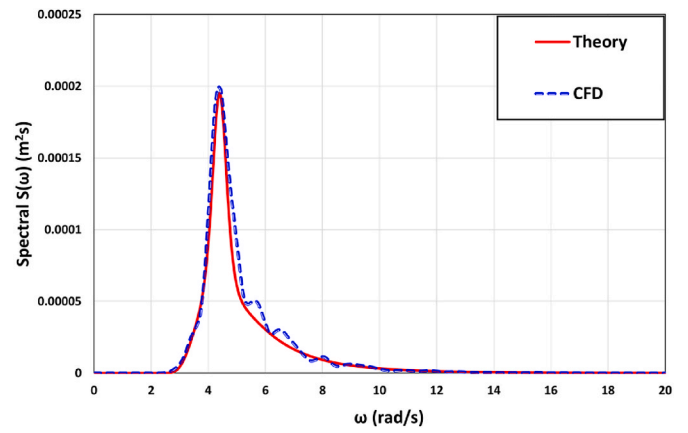

Fig. 10. The comparison of the wave spectrum between the theoretical JONSWAP spectrum and the CFD results (concerning the irregular head sea condition) for sea state 6 ($H_s = 0.0665$m and $T_p = 1.43$s).

elevation displayed in the figure (a sampling frequency of 400 Hz) to produce the spectrum of the generated wave in Fig. 10. Once the wave spectrum is determined, all statistical wave parameters can be derived by using the spectral technique. The nth order spectral moment can be written by

$$m_n = \int_0^\infty \omega^n S_J(\omega) d\omega \qquad (15)$$

in which ω is the incident wave frequency, $S_J(\omega)$ is the JONSWAP spectrum. The square root of the zeroth spectral moment multiplied by

Table 3
Wave characteristics in the validation study.

	Significant wave height	Average wave height	Average wave period
	H_s (m)	$\overline{H}$ (m)	$\overline{T}$ (s)
Theory (JONSWAP spectrum)	0.0665	0.0407	1.20
The Current CFD (Spectral analysis)	0.0695	0.0434	1.22
Error (% of theory)	4.51	6.63	1.66

Fig. 9. The time history of wave elevation for the irregular head sea condition at the numerical wave probe.

4, i.e., $4\sqrt{m_0}$, corresponds to the significant wave height (H_s), which describes the average height of the highest one-third of all waves measured. $2.5\sqrt{m_0}$ and $2\pi\frac{m_0}{m_1}$ represent the average wave height ($\overline{H}$) and period ($\overline{T}$). The critical wave characteristics obtained by the spectral analysis are given in Table 3 and are compared to those calculated from the theoretical JONSWAP spectrum. From Table 3, it can be found that for the statistical quantities of waves, the current CFD model showed differences ranging from 1.66 to 6.63% of the theoretical values. Considering the current cell size and time step, these differences were seen to be acceptable, and the wave generation to be performed for manoeuvring simulations can be claimed to be reasonably validated.

The numerical simulation of the open water characteristics was performed to ensure that the thrust and torque generated by the actuator disk were appropriately estimated. The resulting open water curves are displayed in Fig. 11 in a dimensionless form, where K_T is the thrust coefficient, K_Q is the torque coefficient, η_0 is the open water efficiency, and J is the advance coefficient. It can be seen from the figure that the propeller characteristics simulated by the actuator disk are in satisfactory agreement with the experiments, although the thrust and torque were slightly underpredicted in a regime of high propeller load (errors up to about 6.6% and 5.7%, respectively). The results demonstrated that the actuator disk approach used in the current CFD model is capable of predicting the propeller characteristics with regard to thrust and torque performance. The actuator disk approach was also successfully used in the authors' previous studies (Kim et al., 2021a, 2021b, 2021c, 2022). It should be noted that the propeller effects simulated by the disk model can be decisive for the correct prediction of the manoeuvring response of the ship.

Unfortunately, there are no available experimental results for the KCS's manoeuvrability in long-crested irregular waves of different directions in the literature, such that a comparison could not be made in this paper. However, the authors' previous work (Kim et al., 2021c) performed an extensive validation analysis in terms of kinematic and critical manoeuvring parameters using the present CFD model. It can be seen from their results that the time histories of hydrodynamic features experienced by the manoeuvring ship in both calm and regular seas are well predicted, in particular for surge and yaw velocities and pitch and heave motions being in excellent agreement with experiments. The agreement is also reasonable for the predicted ship trajectories during the turning circle manoeuvre. Given this, it can be argued that the current CFD model enables the reliable prediction of the manoeuvring

capability of the ship in question.

In the authors' previous work (Kim et al., 2021c), a series of grid-spacing and time-step convergence studies were also performed to quantify the numerical uncertainty of the present CFD model for a similar manoeuvring problem in regular waves. Their convergence studies reported that numerical uncertainties for the computed advance, transfer, and tactical diameter were predicted to be a maximum of 0.28% in the spatial convergence study and 0.19% in the temporal convergence study, indicating an acceptable convergent level for ship manoeuvrability simulations in regular waves.

3.2. Course keeping control

In general, ships navigate in open sea areas or restricted waters in accordance with the voyage plan executed and monitored by a master mariner and navigation officer on board. A navigation route in the voyage plan is divided into multiple straight-line segments, each of which is numbered with the true course between two consecutive waypoints. In the practice of navigation, the true course can usually be regarded as the target heading angle to be set as input in the auto-pilot system, such that course keeping control can be identical to automatic heading control, as shown in Wang et al. (2017); (Kim et al., 2021c). It has been observed in real operations that ships inevitably experience deviations from their planned course during course keeping manoeuvres due to the presence of external disturbances such as winds, waves, and currents. Such deviations can involve the risk of serious maritime incidents like collision and grounding, and thus it is considered essential to fully understand the behaviour of a vessel under course keeping control, in order to ensure safe navigation at sea.

As mentioned previously, the self-propulsion computation was initially carried out for all cases. During the computation, the ship experienced an acceleration phase to attain the approach speed along with the development of the boundary layer and wave field. The course keeping manoeuvres were performed from the stable state of self-propulsion condition, letting the ship free to move in 6 degrees of freedom and executing the rudder based on the PID controller.

To evaluate the course keeping capability, the true course (the target heading angle ψ_c) was set at 000° throughout all the course keeping manoeuvres. Fig. 12 presents the time histories of the yaw angle and rudder deflection under the course keeping manoeuvres for all cases. In agreement with the coordinate frames defined in this study, a positive yaw angle indicates the direction of rotation to starboard whilst a negative yaw angle refers to the direction of rotation to port. The rudder angle is positive when turning to starboard while making the ship's heading to port, and a negative rudder angle means the rudder deflection for making the ship's heading to starboard. It can be easily seen from the figure that the rudder deflection became remarkably larger when the ship was moving forward in the irregular bow (Case 2) and regular bow seas (Case 4), i.e., oblique waves. This means that oblique incident waves make the ship's heading control more challenging. The reason for large rudder deflections is closely related to the asymmetric pressure distribution acting on the hull generated by oblique waves, resulting in a substantial yaw moment and thus the heading angle deviation from the target one. The advancing ship in the irregular bow sea experienced the randomly varying behaviour of the yaw and rudder angle during the course keeping manoeuvre, different from that identified in the regular bow sea. This is due to the irregularity in wave height and period based on the JONSWAP spectrum. The maximum rudder deflection in irregular and regular bow seas was observed to be approximately 11.5° and 5.9°, respectively.

Unlike the oblique wave conditions (Case 2 and 4), it was found that the heading control in the irregular head (Case 1), regular head (Case 3), and calm seas (Case 5) was not an issue. In other words, very small heading deviations were observed with less than 0.5° during the course keeping manoeuvre. This mainly resulted from the symmetric pressure distribution on the hull, which hardly caused the yaw moment to make
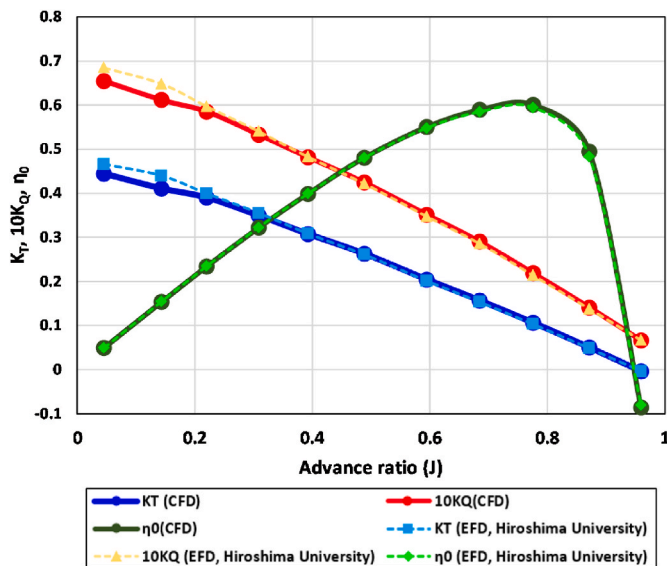

Fig. 11. Open water curves for the KCS propeller model. Solid lines: CFD, Dash lines: Hiroshima university EFD.
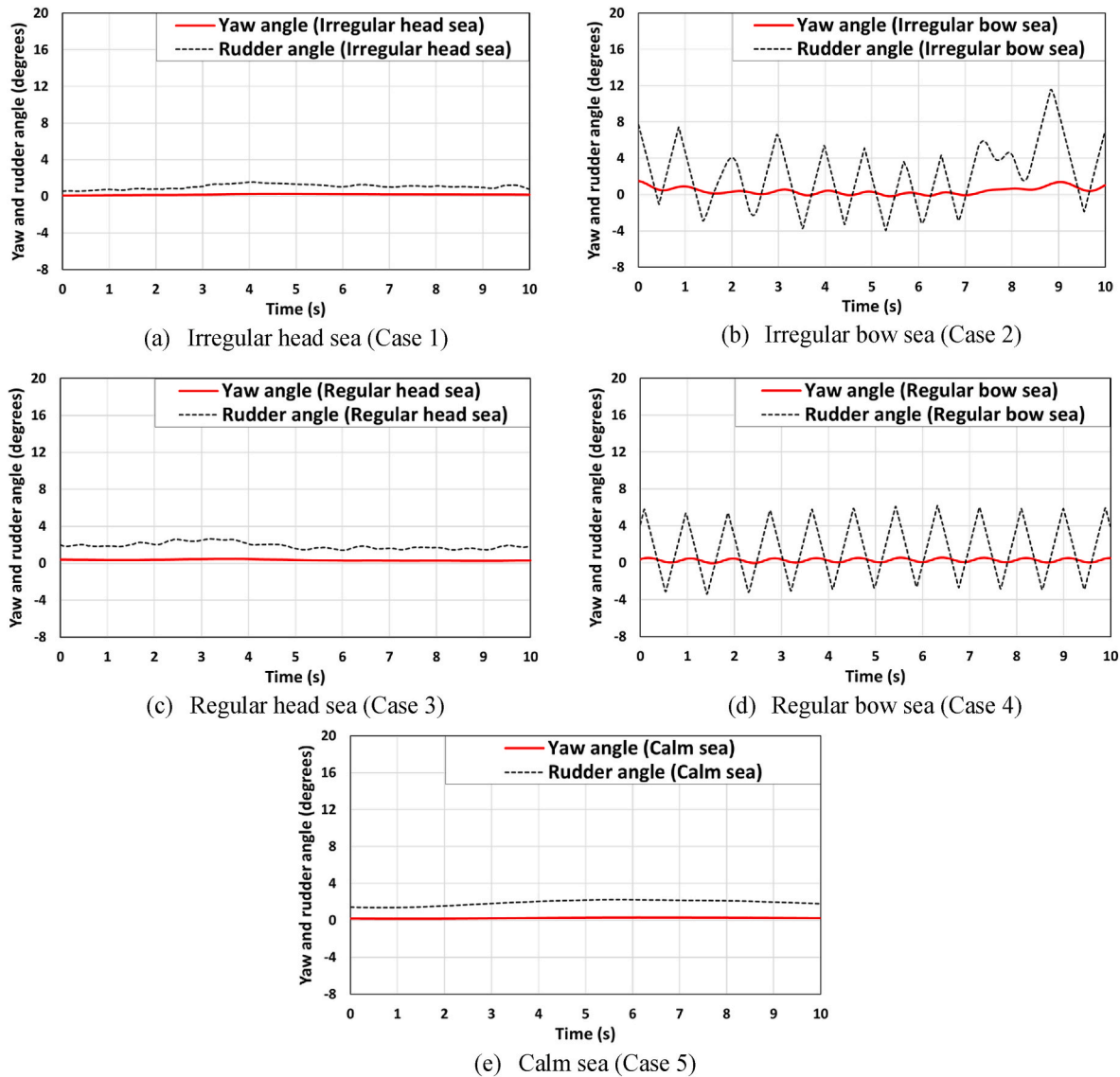
Fig. 12. The time histories of the yaw angle and rudder deflection during the course keeping manoeuvre.

the ship turn. It is important to note that despite the irregularity in wave height and period, heading deviations rarely occurred in the irregular head sea, which implies that the wave coming from the ship's bow can be the desired environmental condition for course keeping control. It is also worth noting that in Cases 1, 3, and 5, small rudder deflections towards the port side were observed within a value of 2.5° when the ship was advancing. Such small deflections were closely correlated to the intrinsic nature of a right-handed propeller, i.e., a non-uniform flow generated by the propeller. To give an example, Fig. 13 presents the snapshots of the longitudinal flow velocities around the rudder and the pressure distribution on the rudder blade during the course keeping manoeuvre. It can be noticed from the figure that the rudder surface is in the slipstream of the actuator disk model, experiencing the flow acceleration. The flow velocity on the port side of the rudder is slightly larger than that on the starboard side when the vessel was sailing forward with the neutral rudder angle. This is due to the non-uniform flow induced by the disk model, resulting in the pressure difference between the starboard side and the port side of the rudder. This uneven pressure exerted a small rudder lift force directed towards the port and thus led to the yaw moment to turn the ship's heading to the starboard side to a small extent. To counterbalance the undesirable yaw moment, the rudder blade was slightly deflected to the port side. This contribution to the ship's heading

control is clearly evidenced in Fig. 12 (a), (c), and (e).

The trajectories experienced by the ship during the course keeping manoeuvre are depicted in Fig. 14. In the figure, the origin point (0,0) represents the position where the course keeping manoeuvre started. As it can be seen, the advancing ship in the irregular and regular bow seas (Case 2 and 4) exhibited a large deviation from the planned course, considerably biased towards the port side. This can be explained by the strong lateral force induced by the oblique waves, and the resultant paths indicated the relatively poor course keeping ability of the ship. It clearly appeared that the regular bow sea condition showed a poorer course-keeping response when compared with the irregular bow sea condition in terms of ship trajectory drifts. In other words, the difference for the trajectory drift between Case 2 and 4 occurred although the equivalent wave input parameters, i.e., the same average wave height and period, were applied. The possible reason for this difference may stem from the difference in the total incident wave energy (being proportional to the wave height squared) experienced by the ship during the course keeping manoeuvre. In addition, the oblique seas (i.e., the irregular and regular bow seas) commonly led to obvious oscillations for the trajectories because of the rudder behaviour with short-term oscillations (Fig. 12 (b) and (d)). On the other hand, good course-keeping control was achieved with a very small deviation by the advancing
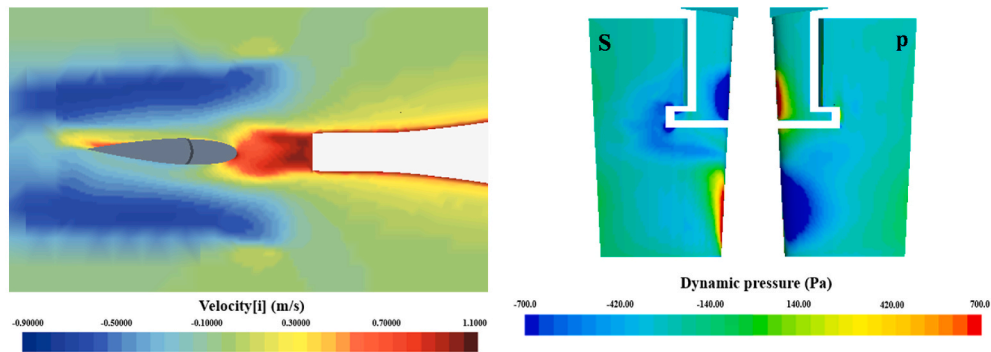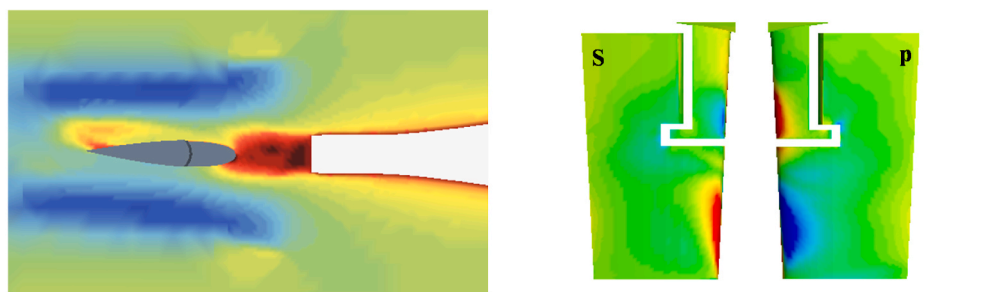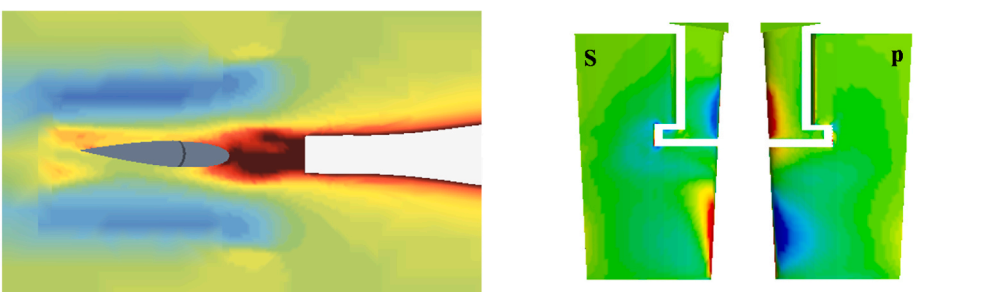
(a) Irregular head sea (Case 1)
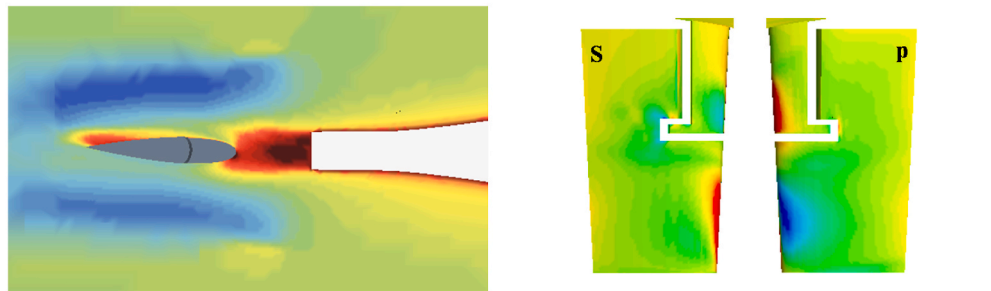
(b) Irregular bow sea (Case 2)
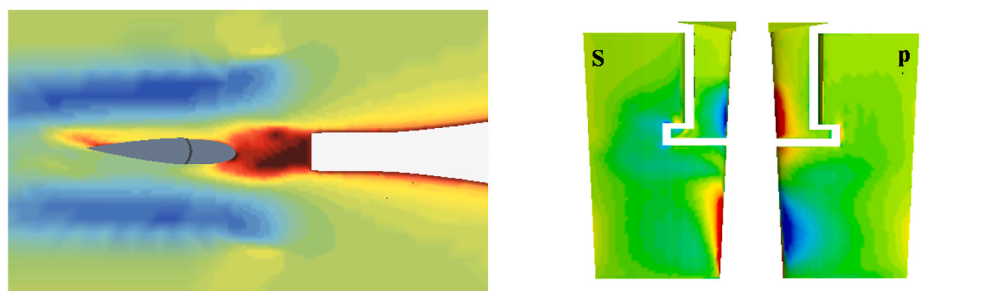
(c) Regular head sea (Case 3)

(d) Regular bow sea (Case 4)

(e) Calm sea (Case 5)

Fig. 13. The snapshots of the axial flow velocities around the rudder (left column) and the pressure distribution on the rudder (right column, S: starboard profile, P: port profile) during the course keeping manoeuvre.
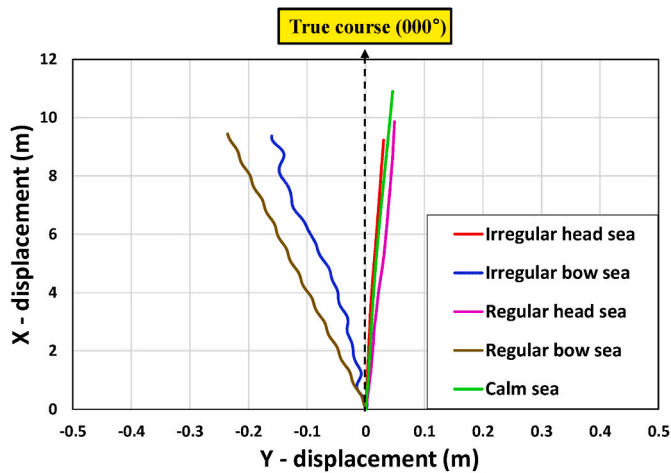
Fig. 14. The comparison of the predicted trajectories for all cases.

ship in the irregular head, regular head, and calm seas. This is intimately related to the very small heading deviation caused by the non-uniform flow. It has to be pointed out that the steering capability can be further improved by applying the optimum gains to mitigate the deviation from the original course.

In order to visualise the wave contours generated by the presence of the ship under course keeping control, the snapshots of the free surface wave elevations for all cases are presented in Fig. 15. It is clearly seen from the figure that asymmetric wave profiles were generated in the irregular and regular bow seas (Case 2 and 4), which resulted in a large lateral force and yaw moment. When the ship was moving forward in the oblique waves, the free surface elevation on the starboard-bow side was higher than that on the port-bow side (Fig. 15 (b) and (d)). As expected, symmetric wave profiles around the ship were observed for the other cases (Case 1, 3, and 5), which can barely cause the lateral force and yaw moment.

3.3. Turning circle manoeuvre

In this sub-section, the turning ability of the KCS model in each simulation will be presented in detail and the results will then be compared to each other. It has to be mentioned that this section dealt with the turning manoeuvres with only the yaw angle variation of 360° based on the guidelines (IMO, 2002a). The turning circle manoeuvres were restarted from the self-propulsion conditions, deflecting the rudder blade to a maximum of 35° (towards the starboard side). The total simulation running time (to complete 360° turns) including the acceleration phase was approximately 75s for the irregular wave cases (Case 1 and 2), 71s for the regular wave cases (Case 3 and 4), and 100s for the calm water case (Case 5). For each irregular wave case, the time to complete the computation was around 1500 wall clock hours and 60,000 CPU hours with 40 CPU processors. Each regular wave simulation required 14,320 CPU hours with 40 CPU processors, completed in approximately 358 wall clock hours, while the calm water simulation needed 5700 CPU hours with 40 CPU processors to complete the computation.

3.3.1. Time histories during the turning and turning indices

The predicted ship trajectories of the turning circle manoeuvre for all cases are presented in Fig. 16, where each case is indicated with a different colour. In the figure, the fixed point (0,0) is the position at which the rudder blade started to be deflected for the manoeuvre. It appears from Fig. 16 that the irregular and regular wave conditions led to substantial changes in the ship's turning capability when compared to the ship's inherent turning ability in calm water, clearly evidenced by the remarkable differences in the turning trajectory. The contribution of
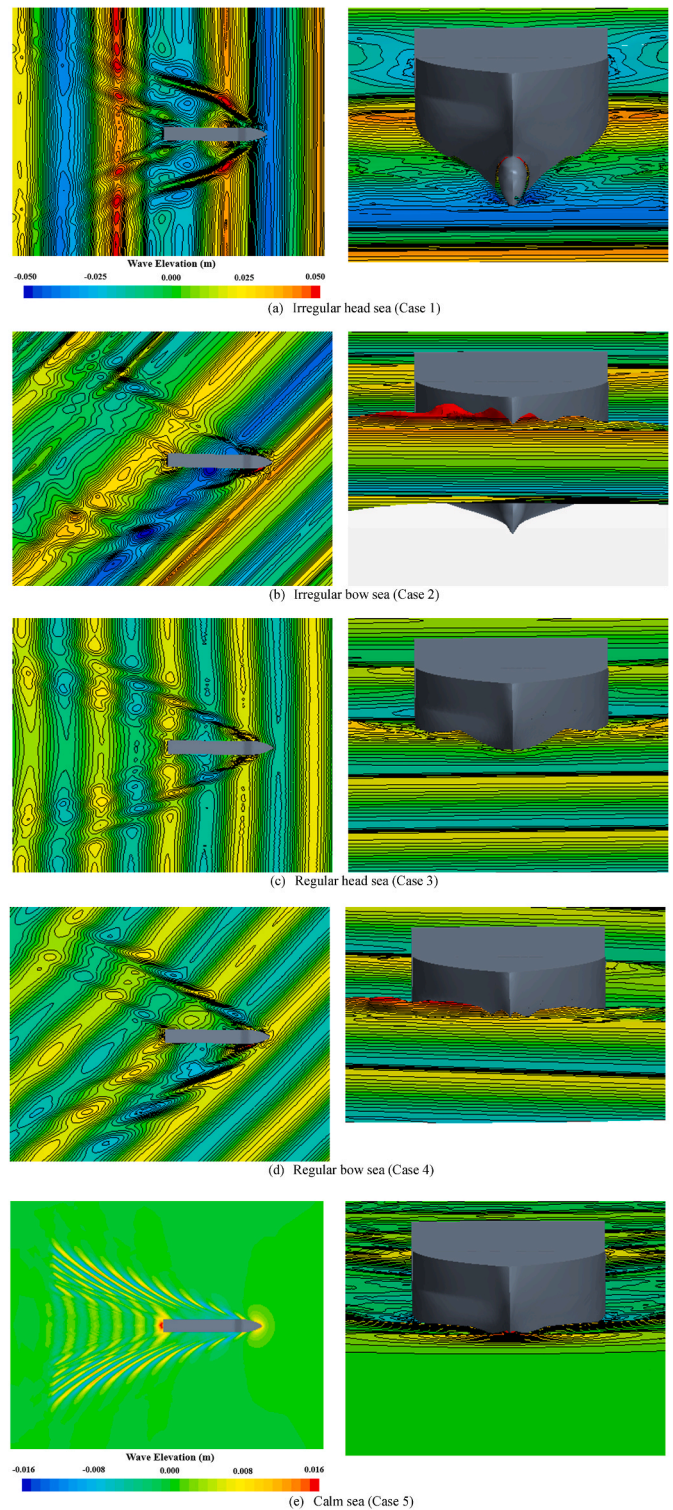

Fig. 15. Measured wave elevation around the KCS hull under course keeping control (left column: top view, right column: front view).

the wave direction to the turning trajectory was also noticed to some extent, confirming the deformation of the turning circle path compared to the trajectory in calm water (due to the wave drift forces and moments). Interestingly, in the case of the same wave direction, the overall trajectory experienced by the ship in the irregular wave was roughly similar to the one observed in the regular wave, exhibiting a similar final position at the end of the manoeuvre.

The critical manoeuvring indices (i.e., the advance, the transfer, the
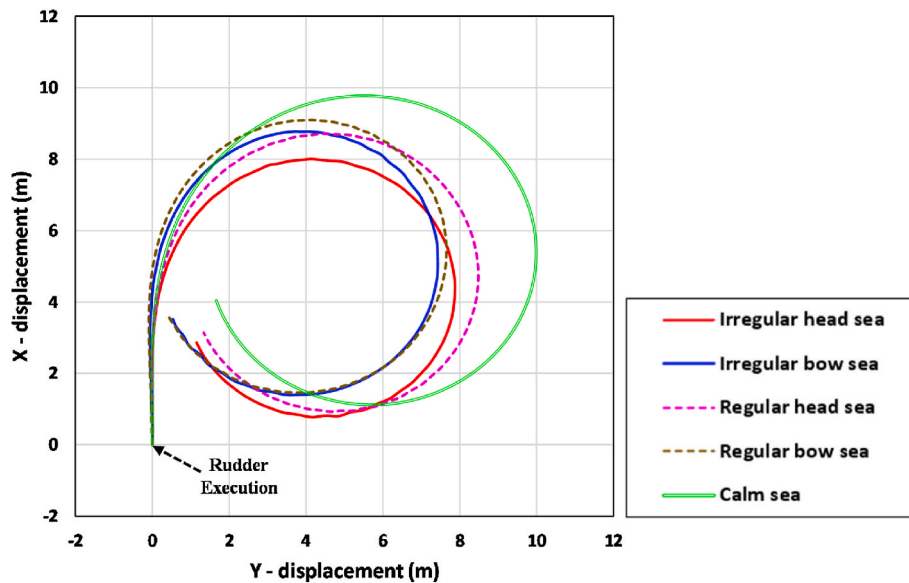
Fig. 16. The turning circle trajectories for all cases.

Table 4
CFD results: turning indices in irregular, regular and calm seas.

Parameters (CFD results)	Case 1	Case 2	Case 3	Case 4	Case 5
Advance (m)	7.78 (2.54 L_{BP})	8.56 (2.80 L_{BP})	8.48 (2.77 L_{BP})	8.86 (2.90 L_{BP})	9.55 (3.13 L_{BP})
Transfer (m)	2.92 (0.95 L_{BP})	2.73 (0.89 L_{BP})	3.26 (1.07 L_{BP})	2.82 (0.92 L_{BP})	4.07 (1.33 L_{BP})
Time for yaw 90° (s)	12.01	12.49	11.69	12.71	12.31
Tactical diameter (m)	7.64 (2.49 L_{BP})	7.25 (2.37 L_{BP})	8.23 (2.69 L_{BP})	7.43 (2.43 L_{BP})	9.82 (3.21 L_{BP})
Time for yaw 180° (s)	22.82	23.60	22.85	23.94	24.20

tactical diameter, and the time to 90°/180° yaw angle change) are summarised in Table 4. The time histories of the predicted ship velocities, forces, and moments during the manoeuvre are shown in Fig. 17 (surge, sway, and yaw parameters with respect to the ship-fixed coordinate and rudder normal force with respect to the rudder-fixed coordinate depicted in Fig. 4). The critical turning parameters are highly dependent on the ship's horizontal motions, namely surge, sway, and yaw motions which are determined by the complex interactions between the hull, propeller, rudder, and environmental loads. Such ship motions have a close correlation with the ship velocities in the horizontal plane (surge, sway, and yaw velocities). In general, the greater the surge speed and the smaller the yaw velocity in the initial transient phase of the turn, the greater the ship advance can be. The maximum ship advance was found to be 3.13L_{BP} in calm water (Case 5), mainly due to the much larger approach speed compared to the wave cases. The advance experienced by the ship in the irregular head sea (Case 1, 2.54L_{BP}) was predicted to be smaller than that in the irregular bow sea (Case 2, 2.80L_{BP}) because of the relatively smaller approach speed and the shorter time taken for 90° turn. The regular bow sea condition (Case 4, 2.90L_{BP}) showed a greater ship advance than the regular head sea condition (Case 3, 2.77L_{BP}) due to the longer time taken for 90° turn, despite the smaller approach speed. It is worth noting that the ship manoeuvring in the irregular head sea (Case 1) achieved a shorter 90° turning time when compared to in the irregular bow sea (Case 2). This

may be ascribed to the wave force and moment acting on the ship during the initial transient phase, resulting in the different increasing trend of the yaw velocity after the rudder deflection (significant fluctuations were noted in the irregular bow sea. In the same manner, the regular head sea condition (Case 3) achieved a shorter 90° turning time than the regular bow sea condition (Case 4). As it can be seen from Fig. 16 and Table 4, the smaller transfer and tactical diameter were achieved by the ship performing the turning manoeuvre in the irregular bow sea condition (Case 2) compared to the irregular head sea condition (Case 1). This may be attributed to the wave drift force acting on the ship in the bow seas, and the contribution to the ship trajectory is clearly evidenced in Fig. 16 (the trajectory drift direction was noted to be similar to the wave propagation direction). In the same way, the ship manoeuvring in the regular bow sea condition (Case 4) experienced the smaller transfer and tactical diameter than the regular head sea condition (Case 3).

It was observed from Fig. 17 that the rudder exerted a strong rudder normal force directed port side as it was actuated in the very early phase of the turn; this lateral force offered the positive yaw moment required to start the starboard turning manoeuvre. Fig. 18, as an example, displays the snapshots of the axial flow velocities around the rudder and the pressure distribution of the rudder according to the rudder deflection angle in the very initial phase of the turn. The pictures are the snapshots obtained from Case 1 (the irregular head sea condition), which can present how the rudder generates the rudder normal force for the ship's turning. From the figure, it clearly appears that as the rudder deflection angle increased, the pressure difference between the starboard and the port of the rudder blade gradually increased. The uneven pressure distributions on the rudder yielded a strong lateral force towards the port side and the resulting yaw moment (positive) enabled the ship to the turning manoeuvre. From Fig. 17, it can be found that the ship experienced an involuntary surge speed loss after the rudder was deflected to a maximum 35-degree angle. This was associated with an increase in the ship resistance caused by a large drift angle. Afterwards, some variations in the forward speed were found according to the wave-encounter condition. Under the wave conditions, a greater increase in the forward speed was obviously observed when the ship encountered the following waves whereas a greater decrease was noted in head seas during the ship's turning. The surge velocities and forces showed high-frequency fluctuations caused by the wave-induced ship motions while the ship was turning in waves, but the fluctuations significantly decreased when the ship experienced the beam waves during the turning manoeuvre. The sway velocities experienced a rapid increase until about
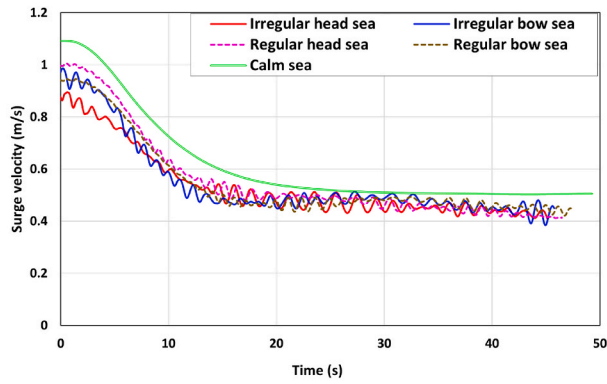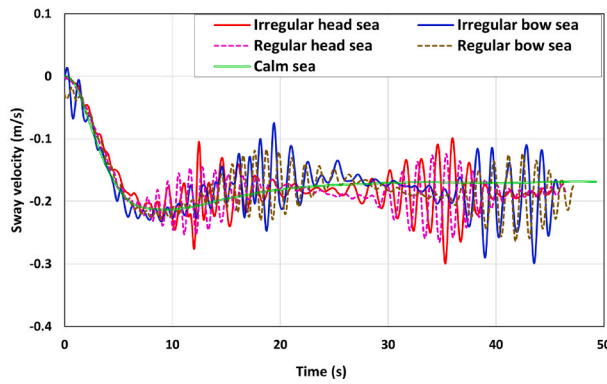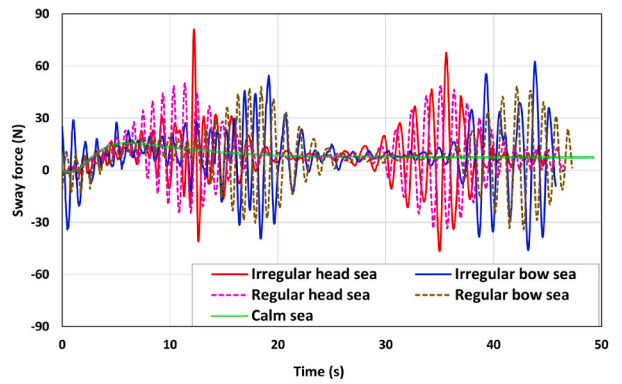
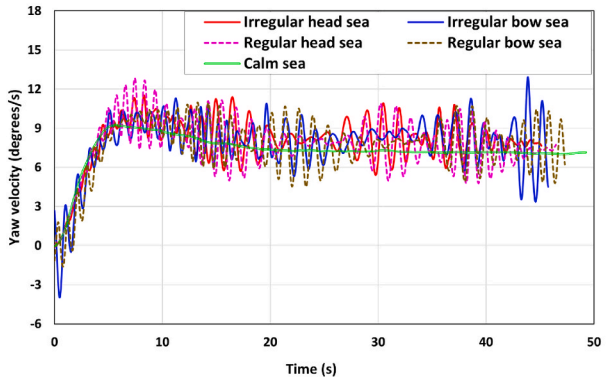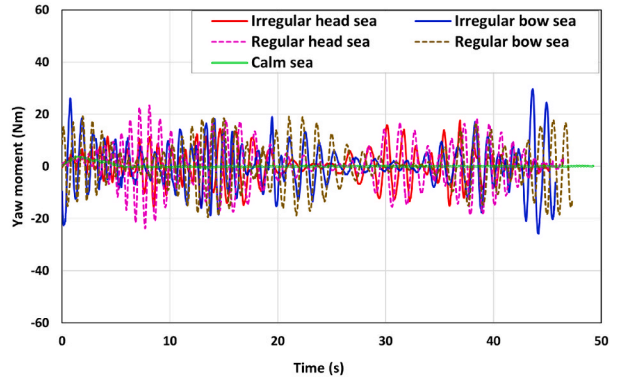(a) Surge velocity
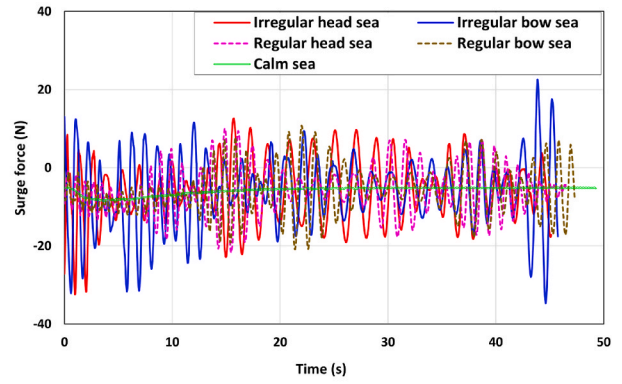
(b) Surge force

(c) Sway velocity

(d) Sway force

(e) Yaw velocity

(f) Yaw moment
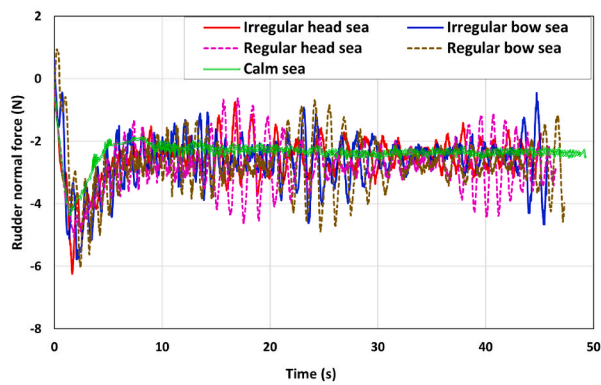
(g) Rudder normal force

Fig. 17. The time histories of the ship velocities, forces, and moments during the ship's turning manoeuvre.

(a) Rudder angle = 0° (t= 0.00s)

(b) Rudder angle = 10° (t= 0.50s)

(c) Rudder angle = 20° (t= 1.00s)

(d) Rudder angle = 30° (t= 1.50s)

(e) Rudder angle = 35° (t= 1.74s)
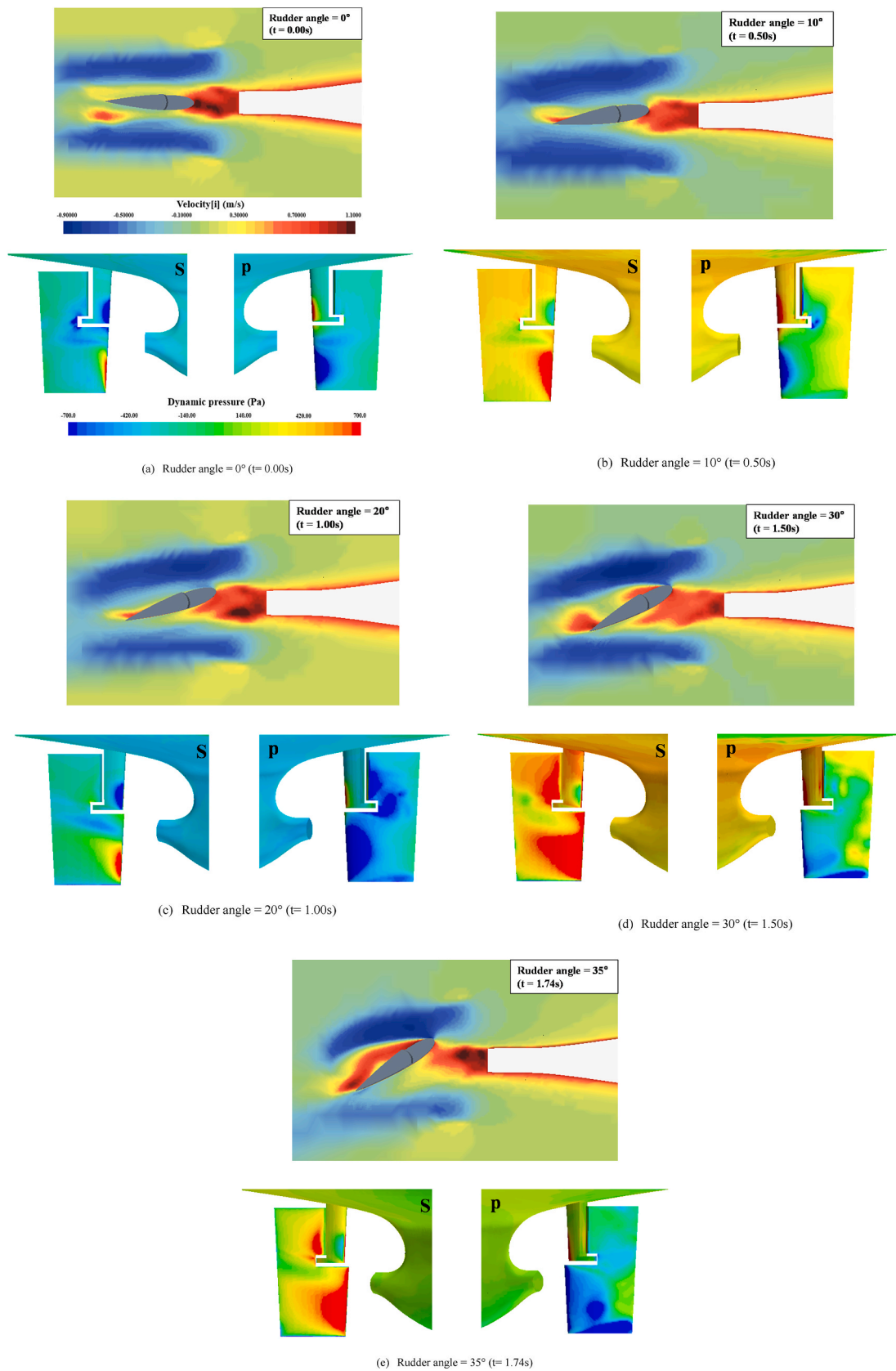
Fig. 18. The snapshots of the axial flow velocities around the rudder and the pressure distribution of the rudder (S: starboard profile, P: port profile) according to the rudder deflection angle in the initial phase of the turning manoeuvre.

7s after the start of the turning manoeuvre and then showed a tendency to converge to between −0.20 m/s and −0.17 m/s with some fluctuations around their average value according to the environmental condition. The sway forces followed the same trend. Unlike the surge velocities and forces, the large fluctuations in the sway velocities and forces were noted when the ship experienced beam seas, whilst the fluctuations almost disappeared under the following seas. The yaw velocities and moments showed the large fluctuations when the ship
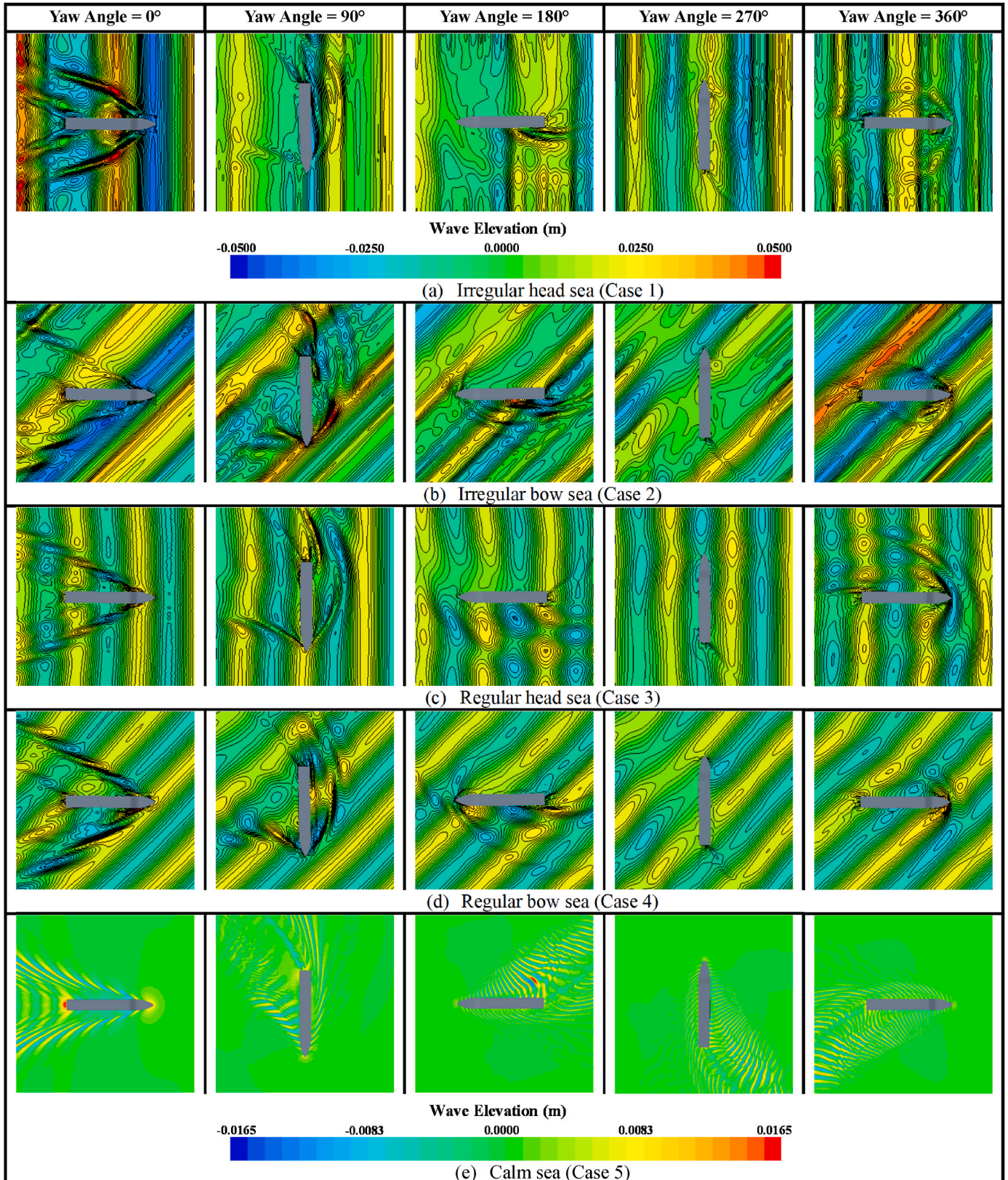

Fig. 19. The free surface elevation during the turning manoeuvre for all cases.

experienced the oblique waves during the ship's turning. The yaw velocities reached maximum approximately 6s after the rudder deflection. Then, they were observed to converge quickly to the values which were estimated at 7.9°/s for Case 1, 8.1°/s for Case 2, 7.3°/s for Case 3, 7.6°/s for Case 4, 7.1°/s for Case 5.

Consecutive views of the free surface elevation around the ship during the turning manoeuvre are reported in Fig. 19. The sequence of the pictures can provide a clear description of the Kelvin waves generated by the ship performing the turning manoeuvre, closely associated with the forward speed and wave-encounter direction during the manoeuvre. The Kelvin wave generated by the ship became more visible when the ship was manoeuvring at a relatively high forward speed (the Froude number is relatively high), which can be clearly seen by the ship operating in the initial phase of the turn (yaw angle = 0° and 90°). It was also observed that the generated Kelvin wave became quite clear when the ship encountered the waves from the ship's bow during the manoeuvre. The free surface was mostly not disturbed much by the ship manoeuvring during the steady phase of the turn (yaw angle = 180°, 270°, and 360°) due to the decreased forward speed (the Froude number is relatively small).

3.3.2. Wave-induced motions during turning manoeuvre

In this sub-section, the seakeeping performance of the ship performing the standard turning manoeuvre is given in detail. The time histories of ship motions, i.e., heave, pitch, and roll as well as relevant hydrodynamic loads acting on the ship are presented in Fig. 20, in which the forces and moments are referred to the ship-fixed coordinate system. It is apparent from the figure that the manoeuvring ship in the irregular waves (Case 1 and 2) mostly experienced the randomly varying responses of the ship motions when compared to the regular sea conditions (Case 3 and 4) due to the irregularity in wave height and period. In addition, instantaneous variations in the ship's velocity and wave-encounter direction during the manoeuvre also seemed to lead to the changes in the motion amplitude and frequency in the waves. For example, the ship manoeuvring in the irregular and regular head seas (Case 1 and 3) encountered the head sea (0° turn), the port beam sea (90° turn), the following sea (180° turn), the starboard beam sea (270° turn), and the head sea (360° turn) in series after starting the starboard turning manoeuvre (the variation in the ship's heading angle is given in Fig. 20 (g)). Given the fact that the ship motions are closely associated with the natural frequency of the motion system, it is obvious that the turning behaviour, which resulted in the continual changes in the wave-encounter frequency, can affect seakeeping performance in waves.

It is quite challenging to provide a clear description of the ship motions during the turning manoeuvre in the irregular seas since they are much more complicated than those predicted in the regular and calm seas. Possible reasons for the increase in the heave and pitch responses while the ship was turning in the irregular seas (Case 1 and 2) include the higher incident wave height and the encounter frequency (f_e) very close to the natural frequency (f_n). Such conditions may cause relatively larger excitation forces and moments. Besides, the heave response appeared to be larger when the ship experienced the starboard or port beam seas, whereas the amplitude of the pitch was predicted to almost disappear under the beam seas (clearly evidenced in Fig. 20 (a) and (c)). The heave and pitch responses in the regular seas (Case 3 and 4) can be understood in a similar manner to the ship motion predictions in the irregular seas. Interestingly, it is clearly seen that during the very initial phase of the turn, the amplitudes of the heave and pitch in the regular head sea were smaller than those predicted in the regular bow sea, which is intimately related to the encountering frequency. In Fig. 21 the time history of the encounter frequencies during the turning manoeuvre in the regular waves is presented. For the present KCS model, a study by Kim et al. (2021c) shows that the natural frequencies of the heaving and pitching system are close to $f_n \approx 0.93$ Hz. The comparison in terms of the encounter frequency confirms that the ship in the regular bow sea experienced the encounter frequency (f_e) closer to the natural frequency

(f_n) at the early phase of the turn. This implies that the excitation force and moment experienced by the ship in the regular bow sea are larger than in the regular head sea. For the calm water case, only small changes in the heave and pitch responses during the manoeuvre were numerically observed due to the absence of external disturbances.

It was found that the turning manoeuvre has a significant influence on the roll response, as clearly seen in Fig. 20 (f). As stated previously, the strong lateral force acting on the rudder blade occurred after the rudder deflection to the hard-over angle (35°). Since the point for force application was located below the centre of mass, the rudder normal force caused the ship to heel to the starboard side (to the centre of the turning circle) right after the rudder execution. Subsequently, the ship started to heel to the port side (to the outside), which may be attributed to the hydrodynamic forces and the centrifugal force acting on the hull. Then, the amplitudes of the roll response gradually decreased and converged to between about 0° and 2° with some fluctuations.

3.3.3. Corrected trajectory

The correction for the drift effect of waves on the turning trajectory experienced by the ship was made in this sub-section, with an aim to estimate the inherent turning trajectory in calm water by using the results measured in wave conditions. According to IMO (2002a), the accurate record of the ship's trajectory, the heading angle, and the elapsed time should be made until at least a 720° turn is achieved to determine the drift velocity induced by external disturbances. To this purpose, the regular sea cases (Cases 3 and 4) were selected as representative cases to exhibit the corrected trajectory. Accordingly, additional computations were carried out for Cases 3 and 4 until the yaw angle variation of 720° was attained; in addition, the turning manoeuvres of the ship with the approach speed corresponding to Cases 3 and 4 were also performed in calm water. Based on the guideline of IMO (2002a), the obtained results after the 180° change of heading were utilised to determine the magnitude and direction of the drift velocity induced by waves in the assumption that the yaw velocity is steady after the 180° turn. In Fig. 22, Positions (x_{1i}, y_{1i}, t_{1i}) and (x_{2i}, y_{2i}, t_{2i}) represent the positions of the ship which have a phase difference of 360°. The local drift velocity $\mathbf{V}_i$ for any two corresponding positions is defined as the follows:

$$\mathbf{V}_i = \frac{(x_{2i} - x_{1i}, \; y_{2i} - y_{1i})}{(t_{2i} - t_{1i})} \tag{16}$$

The estimated mean drift velocity can be calculated as follows:

$$\mathbf{V}_e = \frac{1}{n} \sum_{i=1}^{n} \mathbf{V}_i = \frac{1}{n} \sum_{i=1}^{n} \frac{(x_{2i} - x_{1i}, \; y_{2i} - y_{1i})}{(t_{2i} - t_{1i})} \tag{17}$$

The obtained trajectories in waves can be corrected from the following equation:

$$\mathbf{X}'(t) = \mathbf{X}(t) - \mathbf{V}_e t \tag{18}$$

in which $\mathbf{X}(t)$ is the measured position vector and $\mathbf{X}'(t)$ is the corrected trajectory of the ship ($\mathbf{X}'(t) = \mathbf{X}(t)$ at t = 0).

Fig. 23 displays the corrected trajectories for Cases 3 and 4, calculated in accordance with the approach as described in the above equations. It can be noticed that the drift direction of the ship trajectory during the turning manoeuvre was similar to the wave direction of the incident wave, clearly evidenced by the uncorrected paths coloured with red. It also appeared that the ship trajectories (solid red lines) obtained from the CFD simulations were well corrected such that an exact circular shape of the path (green dashed lines) was obtained. This suggests that the drift effect of waves on the turning trajectory was eliminated for the corrected ones. However, large discrepancies were observed between the corrected trajectories (dashed green lines) and the ones (solid black lines) representing the inherent turning manoeuvrability of the ship in calm water. Possible sources of these discrepancies may mainly result from the difference in the propeller revolution rates applied to the CFD model during the manoeuvre, leading to the difference in the dynamic
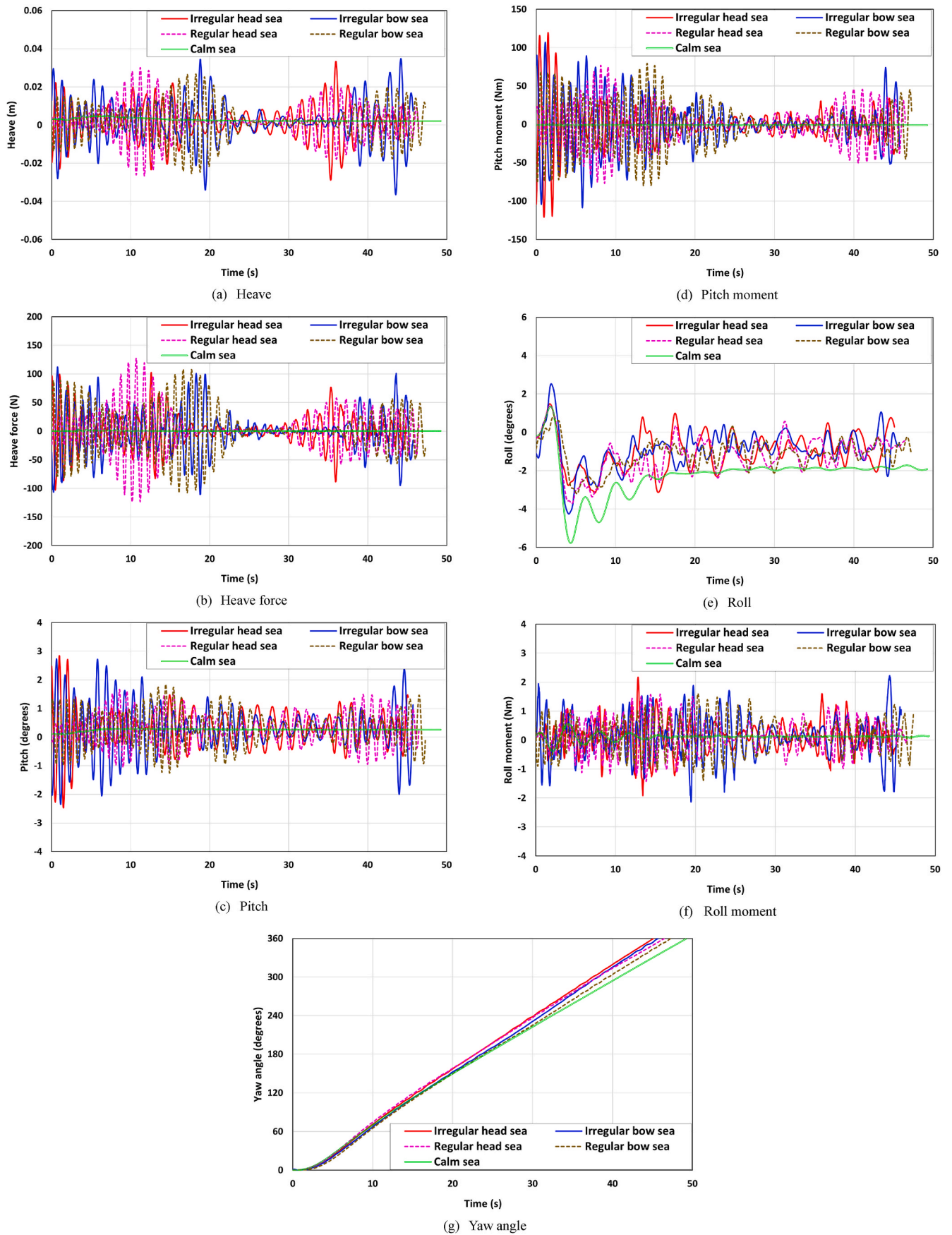
(a) Heave

(b) Heave force

(c) Pitch

(d) Pitch moment

(e) Roll

(f) Roll moment

(g) Yaw angle

Fig. 20. The time histories of ship motions, forces and moments acting on the hull during the turning manoeuvre.
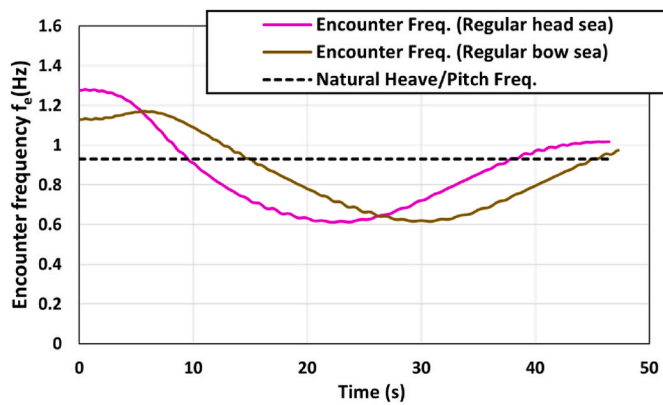
Fig. 21. The time history of the encounter frequencies during the turning manoeuvre in the regular waves.
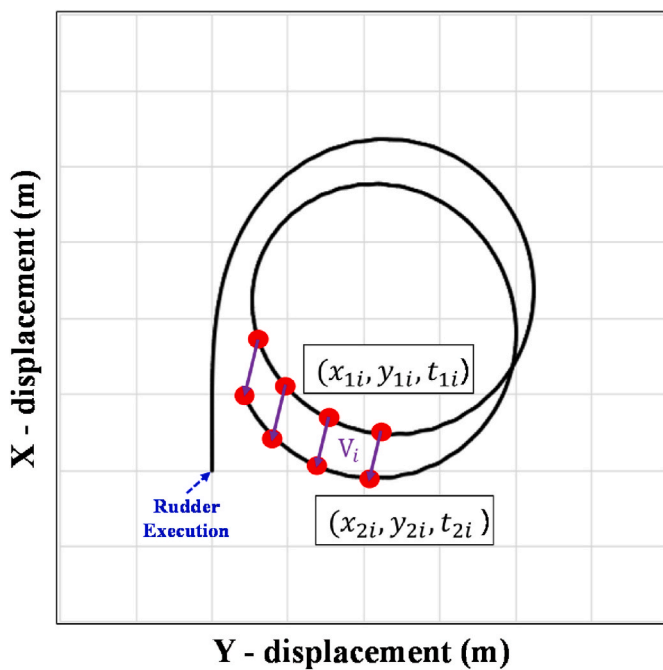

Fig. 22. Turning trajectory in waves.

performance of the ship. This demonstrates the difficulty in predicting the inherent turning trajectory of the ship in calm water through the use of the results obtained in waves to calculate the corrected trajectory.

4. Conclusions and discussion

Free-running simulations to evaluate the course keeping and turning capabilities of a container ship model in irregular waves were performed by means of an unsteady Reynolds Averaged Navier-Stokes solver.

Firstly, it was clearly shown in Section 1 that the past studies published in this area are insufficient to provide a comprehensive description of the ship manoeuvrability in irregular waves. As such, the present study aims to add a sound value by investigating the manoeuvring behaviour of the ship (i.e., course keeping and turning circle manoeuvres) in the irregular waves. Additionally, the comparisons with the ship manoeuvrability in both calm and regular seas were made with the aim of identifying the different manoeuvring behaviours.

Next, a numerical modelling method was proposed to perform free-running CFD simulations of a self-propelled ship in a random wave environment. The detailed explanation of the numerical setup regarding

propeller modelling, mesh generation, time step selection, treatment of computational region motions, and wave modelling was given in the paper.

Following this, before conducting the manoeuvring analyses, a simulation was performed with irregular head waves by generating the static background domain without hull and rudder girds, to monitor and record the wave elevation at the position of the wave probe. It was revealed that the waves simulated using the numerical scheme in this paper gave fairly acceptable results, showing differences ranging from 1.66 to 6.63% of the theoretical values in terms of the statistical quantities of waves (i.e., significant wave height, average wave height, and average wave period).

Following this, five simulation cases, which were composed of irregular, regular, and calm sea conditions, were applied to the container ship model for manoeuvring analyses. It can be noted that a detailed analysis of the course keeping and turning circle manoeuvres was carried out in this work, together with the principal properties of the flow field around the ship. In analysing the correlations between the ship manoeuvrability and the irregular waves, the findings of this study have demonstrated that the irregular waves may cause substantial changes in the course keeping capability and turning performance when compared to the inherent manoeuvring qualities in calm water. The key findings of this work can be summarised as follows:

1) For the ship's heading control in accordance with the prescribed course keeping module, it was identified that the ship operating in the irregular oblique sea experienced larger heading angle deviations than in the irregular head sea. The main reason for this lies in the asymmetric pressure distribution acting on the hull generated by the oblique wave during the course keeping manoeuvre, which resulted in a substantial yaw moment and thus the large heading angle deviation and rudder deflection. In addition, the advancing ship in the irregular bow sea experienced the randomly varying behaviour of the yaw and rudder angle under the course keeping control, clearly different from that identified in the regular bow sea. This is because of the irregularity in wave height and period based on the JONSWAP power spectrum. Unlike the oblique sea cases, it was observed that the heading control in the irregular head, regular head, and calm seas was not an issue, showing very small heading deviations from the target one.

2) It was found that the irregular wave conditions resulted in substantial changes in the ship's turning capability when compared to the ship's inherent turning ability in calm water, showing remarkable differences in the turning trajectory. The influence of the irregular wave direction on the vessels' turning performance was also analysed; for this purpose, the waves of different directions (the irregular head and bow quartering seas) were applied for the evaluation of the ship manoeuvrability. The contribution of the wave direction to the turning trajectory was also noticed to some extent, confirming the deformation of the turning circle path compared to the trajectory in calm water (because of the wave drift forces and moments). An interesting result obtained through this study was that the overall trajectory experienced by the ship in the irregular wave was roughly similar to the one observed in the regular wave (characterised by the height and period equivalent to the average height and period of the irregular waves) in the case of the same wave direction.

It is important to note that the task of ship navigation is to operate the ship from one destination to another as safely as possible in real sea states where the ship is to be navigated. Masters and navigation officers, who are responsible for the navigational operation, are required to fully understand the manoeuvring performance of the ship in a real seaway to ensure navigational safety. It should be borne in mind that inadequate manoeuvring actions by them can result in navigational casualties such as collision, contact, and grounding incidents. There is, however, only limited information available on the ship manoeuvrability under calm
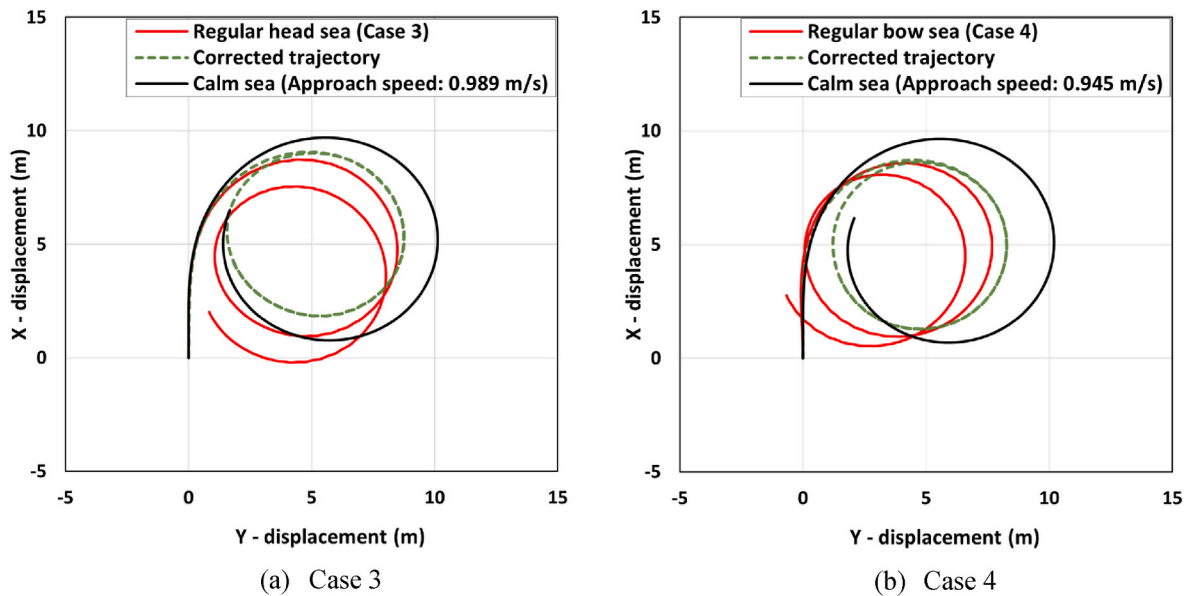
(a) Case 3

(b) Case 4

Fig. 23. The corrected trajectories for Cases 3 and 4.

water conditions, which is generally measured from full-scale sea trials or model-scale tests. Given the fact that such data cannot be informative in confirming the manoeuvring performance in real sea states, it is expected that this work will provide navigators with a deeper insight into the ship manoeuvrability in real sea states as well as support them in proper decision-making for ship handling actions to avoid collision.

It has been observed in real operations that the ship operating in shallow water experiences significant changes in the manoeuvring performance when compared to that in deep water conditions. It is obvious that the ship manoeuvrability in shallow and confined water differs from in deep water due to the interaction between the hull, propeller, and rudder with the bottom surface. In this context, this study could further be extended by investigating the manoeuvring behaviour of the ship in shallow water (in which the available water depth is limited) as a future work, which will contribute to navigational safety.

CRediT authorship contribution statement

Daejeong Kim: Writing – original draft, Conceptualization, Methodology, Formal analysis, Investigation, Validation, Visualization. **Tahsin Tezdogan:** Conceptualization, Methodology, Supervision, Writing – review & editing, Resources, Supervision.

Declaration of competing interest

The authors declare that they have no known competing financial interests or personal relationships that could have appeared to influence the work reported in this paper.

References

Abkowitz, M.A., 1964. Lectures on Ship Hydrodynamics–Steering and Manoeuvrability.
Broglia, R., Dubbioso, G., Durante, D., Di Mascio, A., 2015. Turning ability analysis of a fully appended twin screw vessel by CFD. Part I: single rudder configuration. Ocean Eng. 105, 275–286.

Carrica, P.M., Mofidi, A., Eloot, K., Delefortrie, G., 2016. Direct simulation and experimental study of zigzag maneuver of KCS in shallow water. Ocean Eng. 112, 117–133.
Csp, C.-A., 2021. Personal Corrospondents, Customer Support Portal.
Dubbioso, G., Durante, D., Di Mascio, A., Broglia, R., 2016. Turning ability analysis of a fully appended twin screw vessel by CFD. Part II: single vs. twin rudder configuration. Ocean Eng. 117, 259–271.
EMSA, 2020. Annual Overview of Marine Casualties and Incidents 2020.
Fenton, J.D., 1985. A fifth-order Stokes theory for steady waves. J. Waterw. Port, Coast. Ocean Eng. 111 (2), 216–234.
Ferziger, J.H., Peric, M., 2020. Computational Methods for Fluid Dynamics.
Hasanvand, A., Hajivand, A., 2019. Investigating the effect of rudder profile on 6DOF ship turning performance. Appl. Ocean Res. 92, 101918.
Hasnan, M., Yasukawa, H., Hirata, N., Terada, D., Matsuda, A., 2019. Study of ship turning in irregular waves. J. Mar. Sci. Technol. 1–20.
Hasselmann, K.F., Barnett, T.P., Bouws, E., Carlson, H., Cartwright, D.E., Eake, K., Euring, J., Gicnapp, A., Hasselmann, D., Kruseman, P., 1973. Measurements of Wind-Wave Growth and Swell Decay during the Joint North Sea Wave Project (JONSWAP). Ergaenzungsheft zur Deutschen Hydrographischen Zeitschrift. Reihe A.
IMO, 2002a. Explanatory Notes to the Standards for Ship Manoeuvrability.
IMO, 2002b. Standards for ship manoeuvrability, 137 Resolution MSC 76.
IMO, 2014. 2013 Interim Guidelines for Determining Minimum Propulsion Power to Maintain the Manoeuvrability of Ships in Adverse Conditions.
IMO, 2021. Guidelines for Determining Minimum Propulsion Power to Maintain the Manoeuvrability of Ships in Adverse Conditions.
Inoue, S., Hirano, M., Kijima, K., Takashina, J., 1981. A practical calculation method of ship maneuvering motion. Int. Shipbuild. Prog. 28 (325), 207–222.
ITTC, 2011. ITTC - Recommended Procedures and Guidelines : Practical Guidelines for Ship CFD Applications.
ITTC, 2017a. Recommended Procedures and Guidelines - Seakeeping Experiments.
ITTC, 2017b. Tasks and Structure of 29th ITTC Technical Committees and Groups, version 4.
Kavli, H.P., Oguz, E., Tezdogan, T., 2017. A comparative study on the design of an environmentally friendly RoPax ferry using CFD. Ocean Eng. 137, 22–37.
Kim, D., Song, S., Jeong, B., Tezdogan, T., 2021a. Numerical evaluation of a ship's manoeuvrability and course keeping control under various wave conditions using CFD. Ocean Eng. 237, 109615.
Kim, D., Song, S., Jeong, B., Tezdogan, T., Incecik, A., 2021b. Unsteady RANS CFD simulations of ship manoeuvrability and course keeping control under various wave height conditions. Appl. Ocean Res. 117, 102940.
Kim, D., Song, S., Sant, T., Demirel, Y.K., Tezdogan, T., 2022. Nonlinear URANS model for evaluating course keeping and turning capabilities of a vessel with propulsion system failure in waves. International journal of naval architecture and ocean engineering 14, 100425.
Kim, D., Song, S., Tezdogan, T., 2021c. Free running CFD simulations to investigate ship manoeuvrability in waves. Ocean Eng. 236, 109567.
Menter, F.R., 1994. Two-equation eddy-viscosity turbulence models for engineering applications. AIAA J. 32 (8), 1598–1605.
Menter, F.R., Kuntz, M., Langtry, R., 2003. Ten years of industrial experience with the SST turbulence model. Turbulence, heat and mass transfer 4 (1), 625–632.
Mofidi, A., Carrica, P.M., 2014. Simulations of zigzag maneuvers for a container ship with direct moving rudder and propeller. Comput. Fluid 96, 191–203.

Reynolds, O., 1895. IV. On the Dynamical Theory of Incompressible Viscous Fluids and the Determination of the Criterion (a.). Philosophical transactions of the royal society of london, pp. 123–164, 186.

Romanowski, A., Tezdogan, T., Turan, O., 2019. Development of a CFD methodology for the numerical simulation of irregular sea-states. Ocean Eng. 192, 106530.

Shen, Z., Wan, D., Carrica, P.M., 2015. Dynamic overset grids in OpenFOAM with application to KCS self-propulsion and maneuvering. Ocean Eng. 108, 287–306.

Siemens, 2020. Simcenter STAR-CCM+ Documentation.

Simman, 2020. Workshop on Verification and Validation of Ship Manoeuvring Simulation Methods.

Terziev, M., Tezdogan, T., Incecik, A., 2019. A geosim analysis of ship resistance decomposition and scale effects with the aid of CFD. Appl. Ocean Res. 92, 101930.

Tezdogan, T., Demirel, Y.K., Kellett, P., Khorasanchi, M., Incecik, A., Turan, O., 2015. Full-scale unsteady RANS CFD simulations of ship behaviour and performance in head seas due to slow steaming. Ocean Eng. 97, 186–206.

Wang, J., Wan, D., 2018. CFD investigations of ship maneuvering in waves using naoe-FOAM-SJTU Solver. J. Mar. Sci. Appl. 17 (3), 443–458.

Wang, J., Zhao, W., Wan, D., 2016. Free Maneuvering Simulation of ONR Tumblehome Using Overset Grid Method in Naoe-FOAM-SJTU Solver, 31th Symposium on Naval Hydrodynamics. Monterey, USA.

Wang, J., Zou, L., Wan, D., 2017. CFD simulations of free running ship under course keeping control. Ocean Eng. 141, 450–464.

Wang, J., Zou, L., Wan, D., 2018. Numerical simulations of zigzag maneuver of free running ship in waves by RANS-Overset grid method. Ocean Eng. 162, 55–79.

Yasukawa, H., Yoshimura, Y., 2015. Introduction of MMG standard method for ship maneuvering predictions. J. Mar. Sci. Technol. 20 (1), 37–52.